BMP signaling is required for the generation of primordial germ cells in an insect

Seth Donoughe[a], Taro Nakamura[a], Ben Ewen-Campen[a], Delbert A. Green II[b], Lory Henderson[b], and Cassandra G. Extavour[a,1]

Departments of [a]Organismic and Evolutionary Biology and [b]Molecular and Cellular Biology, Harvard University, Cambridge, MA 02138

Edited by Anthony P. Mahowald, The University of Chicago, Chicago, IL, and approved February 7, 2014 (received for review January 10, 2014)

Two modes of germ cell formation are known in animals. Specification through maternally inherited germ plasm occurs in many well-characterized model organisms, but most animals lack germ plasm by morphological and functional criteria. The only known alternative mechanism is induction, experimentally described only in mice, which specify germ cells through bone morphogenetic protein (BMP) signal-mediated induction of a subpopulation of mesodermal cells. Until this report, no experimental evidence of an inductive germ cell signal for specification has been available outside of vertebrates. Here we provide functional genetic experimental evidence consistent with a role for BMP signaling in germ cell formation in a basally branching insect. We show that primordial germ cells of the cricket *Gryllus bimaculatus* transduce BMP signals and require BMP pathway activity for their formation. Moreover, increased BMP activity leads to ectopic and supernumerary germ cells. Given the commonality of BMP signaling in mouse and cricket germ cell induction, we suggest that BMP-based germ cell formation may be a shared ancestral mechanism in animals.

TGF-β | inductive signaling | Orthoptera | germ line | *piwi*

There are two well-characterized modes of animal germ cell specification. In the inheritance mode, observed in *Drosophila melanogaster*, *Caenorhabditis elegans*, and *Xenopus laevis*, maternally provided cytoplasmic determinants (germ plasm) specify a subset of early embryonic cells as germ cells. In contrast, mice specify their germ line through the induction mode, in which a zygotic cell–cell signaling mechanism specifies germ cells later in development. We previously hypothesized that the inductive mode was ancestral among metazoans and that the inheritance mode had evolved independently in multiple derived lineages (1, 2). Consistent with this hypothesis, multiple basally branching insects do not segregate maternally provided germ plasm, unlike the relatively derived *Drosophila* model (3, 4). However, experimental evidence for the inductive mode was available only for salamanders (5, 6) and mice (7–10), and to date, inferences of induction outside of vertebrates have been based on gene expression and cytological data (1, 11–16).

Because *Drosophila* is highly derived with respect to many aspects of development (17), we examined germ cell development in the cricket *Gryllus bimaculatus*, a basally branching insect that may shed light on putative ancestral mechanisms of specifying germ cells. We previously showed that unlike *Drosophila*, *Gryllus* primordial germ cell (PGC) specification requires zygotic mechanisms rather than germ plasm or the *oskar* germ-line determinant (4, 18). However, the signals that might induce PGC formation in *Gryllus* remained unknown. Because mammals require the highly conserved bone morphogenetic protein (BMP) pathway to specify PGCs (8–10, 19, 20), we investigated BMP signaling as a candidate for regulating inductive germ cell specification in *Gryllus*.

Results and Discussion

Gryllus PGCs first arise among the abdominal mesoderm 2.5 d after egg laying (AEL) (4). To determine whether *Gryllus* PGCs actively transduce BMP signals during their formation, we used multiplex immunostaining to simultaneously detect the PGC marker *Gryllus bimaculatus piwi* orthologue (Gb-Piwi) (4) and the BMP signal effector phosphorylated Mad (pMad) (20). We observed coexpression of high levels of Gb-Piwi and nuclear pMad in mesodermal cells of anterior abdominal segments, revealing that there is active BMP signaling in PGCs at the time that they are specified, and in most PGCs while they coalesce into clusters (Fig. 1 *A–C'''*). We also detected nuclear pMad in both ectodermal and mesodermal cells. This somatic expression was detected at the highest levels laterally (dorsally) and decreased toward the medial (ventral) region, becoming undetectable at 7–10 cell diameters from the lateral (dorsal) edge of the embryo along the entire anterior–posterior axis (Fig. 1 *A–C* and *SI Appendix*, Fig. S2 *A–A'''*). This graded expression pattern is consistent with a conserved role for BMP signaling in dorsoventral patterning (21). The expression of nuclear pMad in PGCs during their formation is also consistent with a role for BMP signaling in PGC specification.

Next, we examined the expression of multiple BMP pathway members in *Gryllus* embryos during PGC formation. *Gryllus* orthologs of vertebrate ligands *BMP2/4* (*Gryllus bimaculatus decapentaplegic*, *Gb-dpp1* and *Gb-dpp2*) and *BMP5/7/8* (*Gryllus bimaculatus glass bottom boat*, *Gb-gbb*) are expressed in the abdomen throughout the period of PGC formation, and are enriched at the dorsolateral margins of the embryo by 4 d AEL (Fig. 1 *D–F'* and *SI Appendix*, Figs. S1 and S2 *D–F'''*). Double labeling of BMP ligand expression and Gb-Piwi (4) confirmed that the BMP ligands *Gb-dpp1* and *Gb-dpp2* are expressed within 2–4 cell diameters of the PGCs (Fig. 1 *D'''–E'''*), and *Gb-gbb* is expressed in cells adjacent to the PGCs (Fig. 1*F'''*). BMP receptors *Gryllus bimaculatus thickveins*

Significance

Many model organisms specify germ cells using maternally supplied germ-line determinants. In contrast, mice rely on embryonic cell–cell signaling to induce cells to become germ cells. Molecular evidence for inductive germ-line specification had previously been provided only for the mouse. Here we provide functional evidence for inductive germ cell specification in an invertebrate, by showing that bone morphogenetic protein (BMP) signaling, which induces mouse germ cell specification, is required for establishment of embryonic germ cells in a cricket. BMP pathway knockdown causes reduction or loss of germ cells, and elevated levels of BMP signaling cause supernumerary and ectopic germ cells. BMP-based germ cell induction in mice and crickets suggests that this may be a shared ancestral mechanism in animals.

Author contributions: S.D., T.N., and C.G.E. designed research; S.D., T.N., B.E.-C., D.A.G., L.H., and C.G.E. performed research; S.D., T.N., B.E.-C., and C.G.E. analyzed data; and S.D. and C.G.E. wrote the paper.

The authors declare no conflict of interest.

This article is a PNAS Direct Submission.

Data deposition: The sequences reported in this paper have been deposited in the GenBank database (accession nos. KF670859–KF670865).

[1]To whom correspondence should be addressed. E-mail: extavour@oeb.harvard.edu.

This article contains supporting information online at www.pnas.org/lookup/suppl/doi:10.1073/pnas.1400525111/-/DCSupplemental.

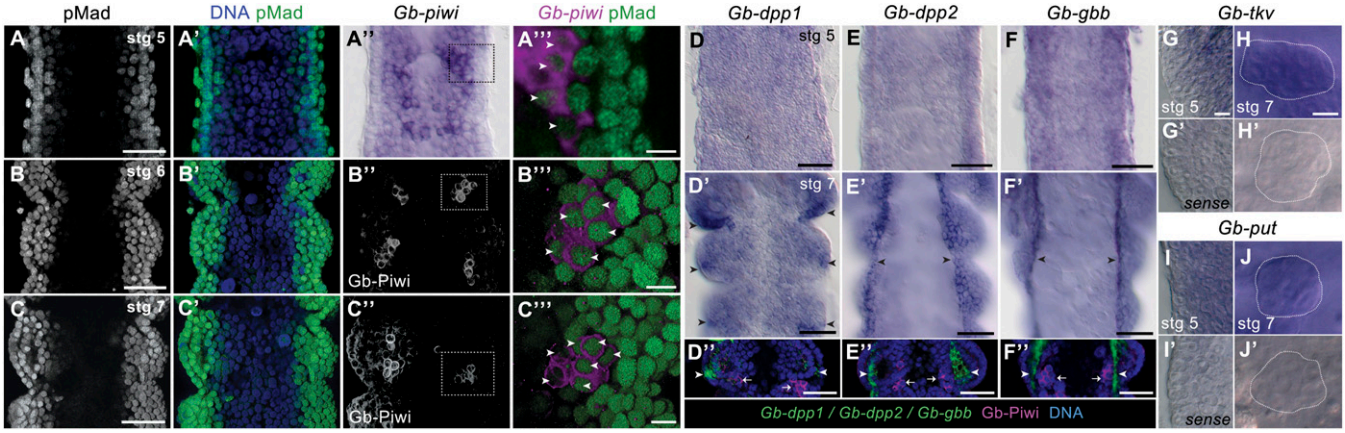

Fig. 1. Expression of BMP pathway components during *Gryllus* PGC formation. (*A–C‴*) Embryos triple stained for nuclei (Hoescht 33342), pMad, and Gb-Piwi at developmental stages 5 through 7, when PGCs are first forming, show that PGCs contain nuclear pMad. Micrographs show single optical sections parallel to the anterior–posterior axis through the dorsal region of anterior abdominal segments, showing the mesoderm flanked by a single layer of ectodermal cells at both lateral margins of the embryo. (*A–C*) Nuclear pMad signal is highest in lateral (dorsal) ectodermal and mesodermal cells and absent from medial (ventral) mesodermal cells. Costaining with *Gb-Piwi* transcripts (*A*) or Gb-Piwi protein (*B* and *C*) reveals nuclear pMad in PGCs. Boxed regions in *A″–C″* are magnified and shown in volume projections in *B‴* and *C‴*. Arrowheads indicate pMad-positive PGCs. As previously documented (4), Gb-Piwi is detectable at the highest levels in PGCs but is also present at lower levels in some mesodermal and ectodermal cells at these stages. (*D–F″*) BMP ligand expression. In stage 5 embryos, *Gb-dpp1* (*D*), *Gb-dpp2* (*E*), and *Gb-gbb* (*F*) are not enriched along the dorsal edge, in contrast to pMad staining (*A*). In stage 7 embryos, *Gb-dpp1* is expressed in ectodermal foci in each segment, and *Gb-dpp2* and *Gb-gbb* are expressed along the dorsal edge of the embryo. Abdominal segments A1–A3 are shown; arrowheads indicate strong ligand expression. (*D″-F″*) Embryos double-stained for BMP ligands (green, indicated by arrowheads) and Piwi protein (magenta, single optical section, indicated by arrows). (*G–J*) Receptors *Gb-tkv* and *Gb-put* are expressed ubiquitously throughout embryogenesis, including in PGCs. (*G*, *G′*, *I*, and *I′*) A dorsal focal plane of stage 5 embryos, where PGCs form. White outlines in *H*, *H′*, *J*, and *J′* indicate PGC clusters in stage 7 embryos. Anterior is up; A2 is the anteriormost segment shown in each panel. [Scale bar, 10 μm in *A‴*, *B‴*, *C‴*, *G*, and *H* (also applies to *G′–J′*), and 50 μm in all other panels.]

(Gb-tkv) (type I) and *Gryllus bimaculatus punt (Gb-put)* (type II) and the BMP effector Smad1/5/8 (*Gryllus bimaculatus Mothers against dpp, Gb-Mad*) are expressed ubiquitously, including in PGCs, throughout PGC specification and cluster coalescence (Fig. 1 *G–J′* and *SI Appendix*, Fig. S2 *B–C″* and *G–J″*). In summary, these expression data indicate that PGCs are competent to receive BMP signals, that BMP ligands are expressed in neighboring and nearby cells and thus could serve as a source of inductive signals, and that PGCs are responding to BMP signals at the time of their specification and throughout subsequent PGC cluster coalescence.

To test for a requirement for BMP signaling in PGC specification, we used RNA interference [RNAi, validated with quantitative PCR (qPCR) and quantification of pMad levels; *SI Appendix*, Fig. S3] to knock down each BMP ligand and the effector *Gb-Mad*. Many BMP pathway RNAi embryos displayed severe morphological defects suggestive of dorsalization, consistent with a conserved role for BMP signaling in dorsoventral patterning (21). However, we also obtained less severely affected RNAi embryos that developed to 4 d AEL, showed normal axial patterning, and possessed all body segments. Despite their generally normal appearance, these embryos displayed reduced pMad levels in the region where PGCs arise (Fig. 2 *L–P* and *SI Appendix*, Fig. S3 *E–L*) and abnormalities in leg development, confirming that BMP signaling was compromised. We quantified PGC defects in these embryos (*SI Appendix*, Figs. S4–S6) and found that 50% of *Gb-Mad* RNAi embryos lacked PGCs ($P < 0.05$, $n = 18$; Fig. 2*C* and *SI Appendix*, Table S3), which was never observed in control embryos ($n = 40$), and the remaining 50% of *Gb-Mad* RNAi embryos had significantly smaller PGC clusters ($P < 0.001$, $n = 180$; Fig. 2*H*) and significantly fewer PGCs than controls ($P < 0.001$, $n = 18$; Fig. 2*A*). Knockdown of BMP ligands also reduced or abolished PGCs, with *Gb-gbb* RNAi embryos showing the most severe phenotype. A total of 30.2% of *Gb-gbb* RNAi embryos lacked PGCs altogether ($P < 0.001$, $n = 43$; *SI Appendix*, Table S3), and the remaining 69.8% of embryos showed significant reduction of PGC cluster size ($P < 0.001$, $n = 430$; Fig. 2 *F* and *K*) and total PGC number per embryo ($P < 0.001$, $n = 43$; Fig. 2*A*). *Gb-dpp1* RNAi resulted in total PGC loss in 12.5% of embryos ($n = 32$; *SI Appendix*, Table S3), and significantly reduced PGC cluster size ($P < 0.001$, $n = 401$; Fig. 2 *D* and *I*) and total PGC number ($P < 0.05$, $n = 32$; Fig. 2*A*) in the remainder. *Gb-dpp2* RNAi embryos did not show a significant decrease in PGC number ($P = 0.67$, $n = 18$; Fig. 2*A*). Consistent with the observation that *Gb-gbb* is expressed in cells closer to the emerging PGCs than either *Gb-dpp* ortholog (Fig. 1*F″*), this suggests that *Gb-gbb* signals may be more important for PGC formation than *Gb-dpp* signals. However, we note that *dpp* signals have been shown to operate across distances of up to 10–15 cell diameters in other organisms (22), consistent with our RNAi data showing that *Gb-dpp1* also contributes to PGC formation, albeit more modestly than *Gb-gbb*. We noted that not all segments of a given embryo were equally severely affected with respect to PGC number: A3 was least affected by *Gb-dpp1* and *Gb-dpp2* RNAi (Fig. 2 *I* and *J*), whereas A2 and A4 appeared marginally less affected than other segments in *Gb-Mad* and *Gb-gbb* RNAi embryos, respectively (Fig. 2 *H* and *K*). These results indicate a requirement for BMP signaling in *Gryllus* PGC development, with *Gb-gbb* likely being the most relevant BMP ligand.

Given that mesoderm is required for *Gryllus* PGC specification (4) and that BMP signaling is required for mesoderm development in many animals (23–27), we considered the possibility that BMP pathway knockdown was disrupting PGC specification indirectly through mesodermal absence or death. At 2.5 d AEL, *Gryllus* mesodermal cells can be unambiguously identified by cellular morphology and anatomical position (28, 29) (*SI Appendix*). We found that in BMP pathway RNAi experiments, embryos at the PGC specification stage (2.5 d AEL) had formed mesoderm correctly (*SI Appendix*, Fig. S7 *A–J′*). Moreover, there was no increase in the number of apoptotic mesodermal cells (*SI Appendix*, Fig. S7*K*). Thus, the loss of PGCs in BMP RNAi treatments is unlikely to be due to a failure of mesoderm specification or death of mesoderm or PGCs. Because it is difficult to quantify *Gryllus* PGCs before PGC cluster formation, we cannot compare PGC proliferation rates directly between RNAi and control embryos.

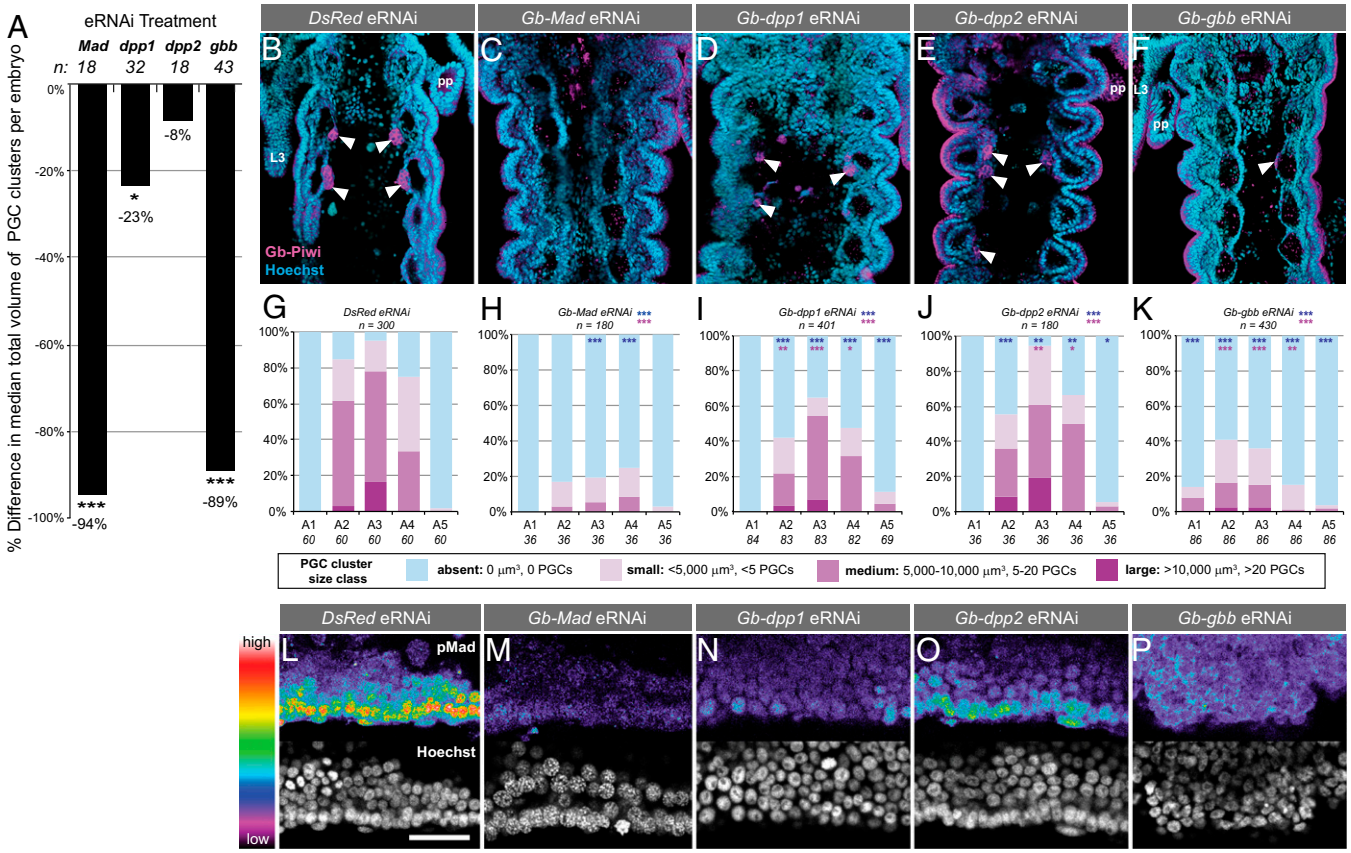

Fig. 2. BMP signaling is required for *Gryllus* PGC specification. RNAi against *Gryllus* BMP pathway members results in loss or reduction of PGCs. (*A*) Percent difference between the median total volume of PGCs clusters per embryo in each knockdown condition compared with controls. (*B–F*) Abdominal segments A1–A5 in a representative embryo from each RNAi treatment at 4 d AEL. PGCs (arrowheads) identified with anti–Gb-Piwi (magenta); anterior is up. (Scale bar, 50 μm.) As previously reported (4), Gb-Piwi expression is also detectable in ectodermal cells at this stage of development. (*G–K*) PGC quantification per segment at 4 d AEL for each BMP pathway RNAi treatment. Blue asterisks indicate significance of presence/absence of PGC clusters compared with controls; pink asterisks indicate significance of size differences of PGC clusters compared with controls. (*L–P*) pMad expression shown with rainbow heat map (white/red, highest levels; purple/black, lowest levels) in the lateral A3 mesoderm at 2.5 d AEL, where PGCs arise, in representative RNAi embryos. Anterior is left. (Scale bar, 50 μm.) Mann–Whitney test significance in *A* and *G–K*, $*P < 0.05$, $**P < 0.01$, $***P < 0.001$.

However, the complete absence of PGCs in a significant proportion of *Gb-Mad* and *Gb-gbb* RNAi embryos and the absence of apoptotic PGCs in all RNAi experiments suggest a direct requirement for BMP signaling in *Gryllus* PGC specification.

We hypothesized that if BMP signaling acts as a direct inductive signal in PGC specification, then elevated or ectopic levels of BMP signaling might increase the number of PGCs formed or cause them to form in ectopic locations. To test this hypothesis, we took two approaches to raise BMP signaling activity in early embryos above wild-type levels: (*i*) injecting 4′-hydroxychalcone, a recently identified chemical activator of the BMP pathway (30), and (*ii*) injecting recombinant *D. melanogaster* Decapentaplegic (Dpp) protein (Dm-Dpp) (*SI Appendix*, Figs. S8 and S9). In both treatments, axial patterning, mesoderm formation, and overall embryonic morphology appeared normal in experimental embryos, but nuclear pMad levels at the time of PGC specification were slightly elevated and expanded toward the ventral midline with respect to controls (Fig. 3 *M–O* and *SI Appendix*, Fig. S10 *A–D*). PGC cluster size showed a dose-dependent increase in every segment of treated embryos (Fig. 3 *D–F′* and *SI Appendix*, Fig. S10*E*). Summing the volumes of all PGC clusters in an embryo showed that the total number of PGCs per embryo was increased by up to 42% (Fig. 3*G*), consistent with activation of BMP signaling. In addition, both treatments caused a significantly increased frequency of ectopic PGCs, defined as PGCs found in segments A1, A5, or A6 (10 mM 4′-hydroxychalcone, $P < 0.01$, $n = 31$, Fig. 3 *E′* and *L*; 10 μg/mL Dm-Dpp, $P < 0.01$, $n = 23$, Fig. 3 *F* and *J–L*; 100 μg/mL Dm-Dpp, $P < 0.05$, $n = 15$, Fig. 3 *F′* and *L*). Ectopic and supernumerary PGCs were not randomly distributed, but instead were clustered adjacent to the coelomic pouches like wild-type PGCs (Fig. 3 *C*, *C′*, *I*, and *K*). Ectopic PGCs are unlikely to result from mismigration, as *Gryllus* PGCs arise in the segments that will house the gonad primordium (A2–A4) and, unlike PGCs in *Drosophila* or mice, do not undergo long-range migration (4). To definitively eliminate the possibility of BMP-induced mismigration, one would need to track PGCs in vivo, a technique that is not currently possible in *Gryllus*.

Some embryos treated with Dm-Dpp displayed an increase in the proportion of A2–A4 segments lacking PGCs (*SI Appendix*, Fig. S10 *F* and *H*). We note, however, that a low level of PGC loss in these segments can be a nonspecific consequence of embryo perturbation, even in buffer-only injected controls, and that the proportion of these segments lacking PGCs in 4′-hydroxychalcone–treated embryos was not significantly different from controls (*SI Appendix*, Fig. S10 *F–H*). We think it unlikely that BMP signaling actively represses PGC formation, as this hypothesis does not explain the supernumerary or ectopic PGCs induced by the BMP activation treatments. However, the altered distribution of PGCs induced by widespread BMP activation suggests that PGC specification is not solely dependent on BMP levels, but instead may involve a range of acceptable BMP signal levels integrated with

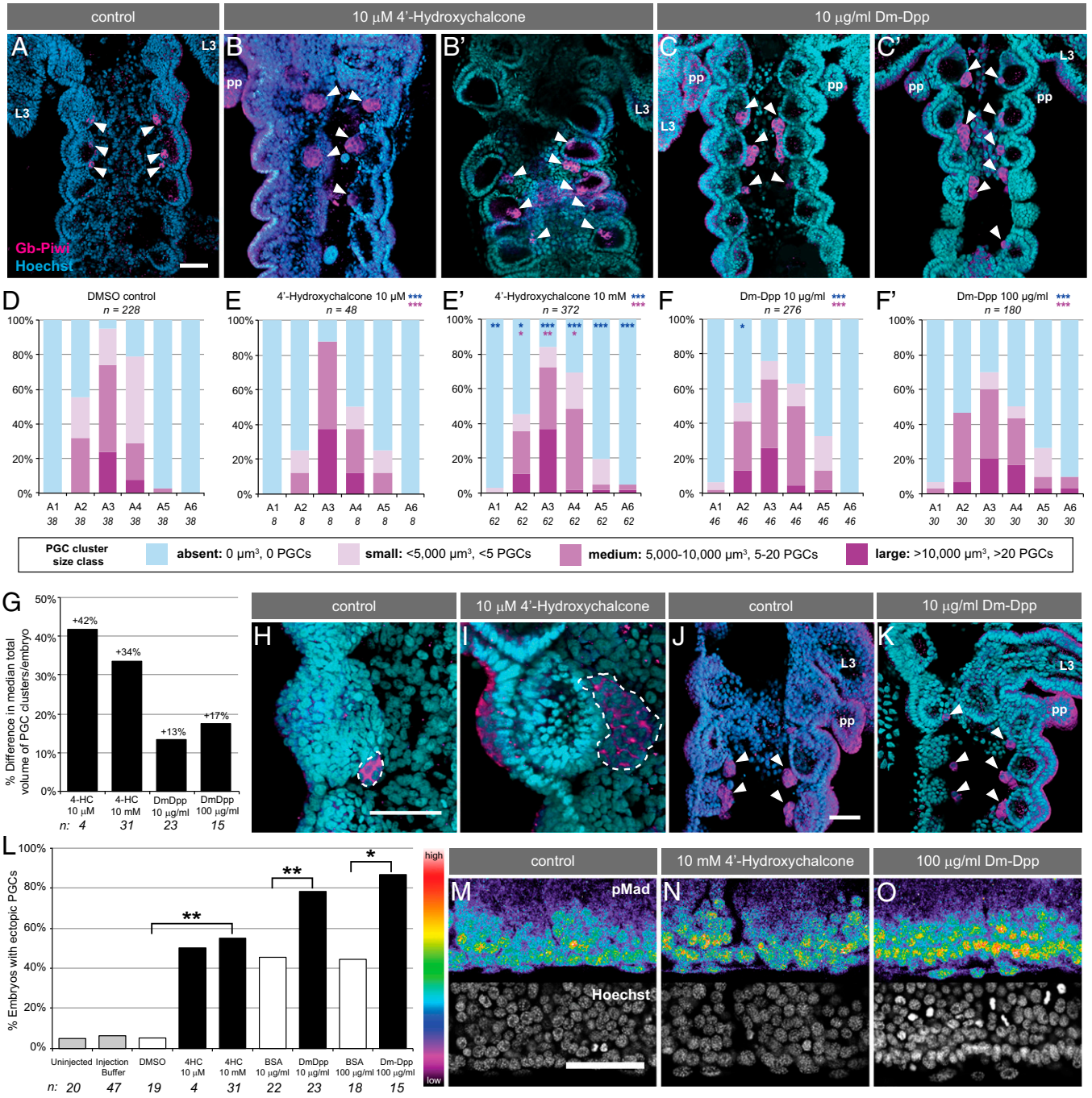

Fig. 3. Elevated BMP signaling levels induce supernumerary and ectopic *Gryllus* PGCs. Abdominal segments A1–A6 from (*A*) a representative DMSO control embryo (BSA controls were similar), (*B* and *B′*) 10 μM 4′-hydroxychalcone–injected, and (*C* and *C′*) 10 μg/mL Dm-Dpp–injected embryos at 4 d AEL. PGCs (arrowheads) identified with anti–Gb-Piwi (magenta); anterior is up. (Scale bar, 50 μm.) L3, third thoracic leg; pp, pleuropodia. A1 is the anterior-most segment in each panel unless otherwise indicated. (*D*–*F′*) Quantification of total PGCs per segment at 4 d AEL in control and experimental embryos. Asterisks indicate significance as described in the Fig. 2 legend. (*G*) Percent difference between median total volume of PGC clusters per embryo in each knockdown condition compared with controls. (*H* and *I*) Higher magnification views of a single PGC cluster (white outline) in a control (DMSO) and a 10 μM 4′-hydroxychalcone–injected embryo. Gb-Piwi expression appears patchy in PGCs because it is localized to the cytoplasm and PGCs have a high nuclear:cytoplasmic ratio (4). (*J* and *K*) Higher magnification views of PGC clusters in a control (10 μg/mL BSA) and 10 μg/mL Dm-Dpp–injected embryos. PGCs are present only in segments A2 and A3 in controls (*J*), but are present ectopically in segment A1 in Dm-Dpp–injected embryos (*K*). (*L*) Quantification of ectopic PGC clusters in BMP-activated embryos compared with controls. Bars represent percent of embryos in each treatment that have at least one ectopic PGC cluster. (*M*–*O*) pMad expression shown with rainbow heat map (white/red, highest levels; purple/black, lowest levels) in the lateral A3 mesoderm at 2.5 d AEL, where PGCs arise, in representative control and BMP-activated embryos. Anterior is left; dorsal margin is down. (Scale bar, 50 μm.) Mann–Whitney test significance in *D*, *E*, *E′*, *F*, *F′*, and *G*–*L*, $*P < 0.05$, $**P < 0.01$, $***P < 0.001$.

additional segment-specific positional information. This hypothesis is additionally consistent with the expression of nuclear pMad during PGC formation (Fig. 1 *A*–*C* and *SI Appendix*, Fig. S2 *A*–*A″*), as the presence of nuclear pMad in some non-PGC cell types suggests that additional mechanisms may be involved in PGC specification. In mice, where BMP signaling induces PGC formation,

phosphorylated SMAD is also detectable in multiple somatic cells, including cells neighboring the nascent PGCs (31). A combination of antagonistic and competence signals operate together with BMP signaling to ensure mouse PGC specification in only a subset of phosphorylated SMAD-positive cells, and we hypothesize that analogous mechanisms may be operative in *Gryllus*. Thus, although we cannot formally rule out additional roles for BMP signaling in migration, maintenance, and/or proliferation of PGCs, we propose that our results are most consistent with the hypothesis that BMP signaling induces PGC specification in *Gryllus*.

We have provided evidence that cricket PGCs are specified via BMP signaling, which appears to be necessary for cricket PGC formation. These data represent, to our knowledge, the first functional genetic evidence for an inductive mode of invertebrate germ cell specification. Our results support a model whereby *Gb-gbb* signals (and to a lesser extent *Gb-dpp1* signals) from the dorsolateral abdominal ectoderm are transduced via *Gb-Mad* in the adjacent mesoderm and cause some of those cells to adopt PGC fate. The presence of supernumerary germ cells in BMP activation experiments and the reduction in PGC cluster size in RNAi experiments raise the possibility that BMP signaling promotes PGC proliferation as well as, or rather than, specification. However, this hypothesis does not account for the presence of ectopic PGCs, given that *Gryllus* PGCs do not undertake long-term migration (4), nor for the complete absence of PGCs in *Gb-gbb* and *Gb-Mad* RNAi experiments, given that PGC clusters are derived from a large number of initially specified precursors rather than just one or a few cells (4).

The fact that ectopic germ cells are found only in lateral positions may be because although pMad levels are elevated by both treatments (Fig. 3 *M–O*), the shape of the activation profile is the same as that of wild-type embryos: nuclear pMad is at the highest levels dorsolaterally, where PGCS are specified, and at the lowest levels ventrally, where PGCs are never observed (*SI Appendix*, Fig. S10 *B* and *D*). We hypothesize that an inhibitory ventral signal, possibly of the *sog*/*Chordin* family, may restrict BMP signaling to dorsal tissues. Alternatively or in addition, a lateral competence signal may play a role in ensuring that not all cells expressing high levels of nuclear pMad differentiate as PGCs. With respect to their specification at the correct position along the anterior–posterior axis, the mechanism(s) that restricts PGC formation to the lateral mesoderm of segments A2–A4 in wild-type embryos are currently unknown. The appearance of ectopic PGCs anterior and posterior to wild-type positions in BMP activation experiments suggests that sufficiently high BMP signaling activity may perturb or overcome the positional information, potentially *Hox* gene-mediated, that normally limits PGC specification along the anterior–posterior axis. Our observation of segment-specific effects on PGC number in both the RNAi and BMP activation experiments is consistent with this model, as it suggests that PGC sensitivity to BMP signaling varies along the anterior–posterior axis.

Our findings in the cricket are similar to those observed in mouse PGC specification. In both cases, an ectodermal BMP signal induces a competent subset of mesoderm to become PGCs (32). PGC phenotypes are observable only in mildly knocked down *Gryllus* embryos, or in heterozygous knockout mice (8–10), as strong RNAi phenotypes and homozygous knockout conditions severely disrupt early development. Loss of BMP2/4, BMP8, and SMAD1/5/8 orthologs leads to loss or reduction of PGCs in both systems (Fig. 4*A*). Two parsimonious evolutionary scenarios based on functional genetic data that could explain the mechanistic similarities observed in cricket and mouse PGC specification are that BMP-based PGC induction (*i*) originated in a Bilaterian ancestor (denoted by a red diamond in Fig. 4*B*) or (*ii*) evolved independently within amniotes and insects (red text in Fig. 4*B*). Given that, to our knowledge, a role for BMP signaling in PGC formation has been directly tested in only two phyla, at present it is difficult to determine which of these hypotheses is more likely. However, in support of the first hypothesis, we note that in multiple metazoan phyla, germ cells are responsive to BMP signaling at some stage of their development, including PGC specification, gametogenesis, germ-line stem cell divisions, and adoption of germ cell fate by stem cells in culture (Fig. 4*B* and *SI Appendix*). This suggests that in addition to its conserved role in dorsoventral patterning (21), there is an ancient and widespread association of BMP signaling with germ cell fate or pluripotency. If future studies reveal a role for BMP signaling in PGC formation in additional taxa that use the inductive mode, that

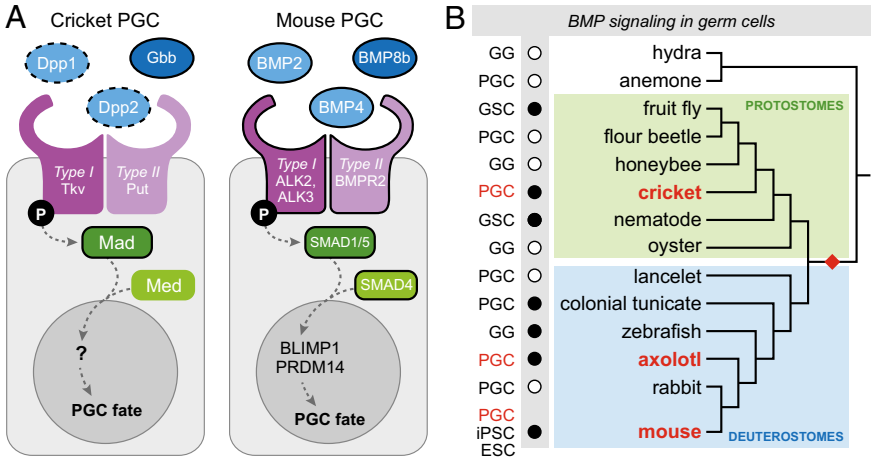

Fig. 4. BMP signaling in germ cells across the Metazoa. (*A*) Hypothetical model for BMP pathway function in cricket and mouse PGCs. Homologous proteins are shown in the same color. Black outlines indicate molecules whose role in germ cells has been tested experimentally through knockdown or knockout experiments; dotted black outline of Gb-Dpp orthologs indicates a potentially minimal or absent requirement in PGC specification. Ligand–receptor interactions are schematized only, as the specific interactions are unknown for both systems. (*B*) Phylogenetic distribution of animals for which expression (white circles) or functional (black circles) data suggest that BMP signaling is involved in some aspect of germ cell development (*SI Appendix*): ESC, conversion of embryonic stem cells to germ cells; GG, gametogenesis; GSCs, germ-line stem cells; iPSC, conversion of induced pluripotent stem cells to germ cells; PGCs, primordial germ cells. Red text indicates animals for which functional data support a role for BMP signaling in PCG specification; these data could support a hypothesis of convergent evolution of BMP-based germ cell formation in two or more bilaterian clades. Red diamond indicates the hypothesis of an ancestral role for BMP signaling in bilaterian PGC formation.

would further support the hypothesis that BMP signaling constitutes an ancestral animal mechanism for specification of the germ line.

Materials and Methods

Genes were cloned using sequences from the *Gryllus* developmental transcriptome (33), with additional sequence data kindly provided by T. Mito (University of Tokushima, Japan). All sequences reported in this study have been deposited in GenBank under accession nos. KF670859–KF670865. *Gryllus* culturing, phylogenetic analysis, in situ hybridization, immunostaining, dsRNA synthesis, and qPCR were conducted as previously described (4). Zygotic RNAi was achieved by injection of dsRNA at either 0–5 h AEL or 24–36 h AEL using previously described injection techniques (4). Small molecule activation of the BMP pathway was accomplished by injecting eggs at 0–5 h AEL with (*i*) either 10 μM or 10 mM of 4′-hydroxychalcone (30) (Santa Cruz Biotechnology Chemicals SC-262260) in DMSO, with DMSO as a control, and (*ii*) either 10 μg/mL or 100 μg/mL of recombinant Dm-Dpp protein (R&D Systems 159-DP-020/CF) in dilute HCl as per the manufacturer's instructions, with 10 or 100 μg/mL of BSA in dilute HCl as a control. To quantify PGCs, the volume of each PGC cluster at 4 d AEL was calculated as an ellipsoid with confocal micrographs of optical sections through the region of the abdomen containing germ cells (*SI Appendix*, Fig. S4). The volume of each PGC in a cluster was both independent of the number of PGCs in a cluster and unaffected by BMP RNAi treatments. The calculated volume of a whole PGC cluster was thus strongly positively correlated with the number of PGCs in that cluster. Measurements of PGC cluster volume, which were more efficient than directly counting PGCs, therefore allowed us to accurately determine the total number of PGCs per cluster, per segment, and per embryo.

ACKNOWLEDGMENTS. We thank T. Mito for the *Gb-dpp2* sequence; D. Vasiliauskas, S. Morton, T. Jessell, E. Laufer, and S. Kunes for reagents; A. Ahuja for discussion of statistical analysis; and W. Gelbart, M.H.T. Extavour, and Extavour lab members for discussion. This research was supported by National Science Foundation (NSF) Grants IOS-1257554 and IOS-1257217 (to C.G.E.), a Ford Foundation Dissertation Fellowship (to D.A.G.), and NSF Graduate Training Fellowships (to S.D., D.A.G., and B.E.-C.).

1. Extavour CG, Akam ME (2003) Mechanisms of germ cell specification across the metazoans: Epigenesis and preformation. *Development* 130(24):5869–5884.
2. Extavour CG (2007) Evolution of the bilaterian germ line: Lineage origin and modulation of specification mechanisms. *Integr Comp Biol* 47(5):770–785.
3. Ewen-Campen B, Jones TE, Extavour CG (2013) Evidence against a germ plasm in the milkweed bug *Oncopeltus fasciatus*, a hemimetabolous insect. *Biol Open* 2(6): 556–568.
4. Ewen-Campen B, Donoughe S, Clarke DN, Extavour CG (2013) Germ cell specification requires zygotic mechanisms rather than germ plasm in a basally branching insect. *Curr Biol* 23(10):835–842.
5. Nieuwkoop PD (1951) Experimental observations on the origin and determination of the germ cells, and on the development of the lateral plates and germ ridges in the urodeles. *Arch Neerl Zool* 8(1):1–205.
6. Sutasurya LA, Nieuwkoop PD (1974) The induction of the primordial germ cells in the urodeles. *Wilhelm Roux' Archiv* 175(3):199–220.
7. Tam PP, Zhou SX (1996) The allocation of epiblast cells to ectodermal and germ-line lineages is influenced by the position of the cells in the gastrulating mouse embryo. *Dev Biol* 178(1):124–132.
8. Lawson KA, et al. (1999) *Bmp4* is required for the generation of primordial germ cells in the mouse embryo. *Genes Dev* 13(4):424–436.
9. Ying Y, Liu XM, Marble A, Lawson KA, Zhao GQ (2000) Requirement of *Bmp8b* for the generation of primordial germ cells in the mouse. *Mol Endocrinol* 14(7):1053–1063.
10. Ying Y, Zhao GQ (2001) Cooperation of endoderm-derived BMP2 and extraembryonic ectoderm-derived BMP4 in primordial germ cell generation in the mouse. *Dev Biol* 232(2):484–492.
11. Juliano CE, et al. (2006) Germ line determinants are not localized early in sea urchin development, but do accumulate in the small micromere lineage. *Dev Biol* 300(1): 406–415.
12. Brown FD, et al. (2009) Early lineage specification of long-lived germline precursors in the colonial ascidian *Botryllus schlosseri*. *Development* 136(20):3485–3494.
13. Kawamura K, et al. (2011) Germline cell formation and gonad regeneration in solitary and colonial ascidians. *Dev Dyn* 240(2):299–308.
14. Agee SJ, Lyons DC, Weisblat DA (2006) Maternal expression of a NANOS homolog is required for early development of the leech *Helobdella robusta*. *Dev Biol* 298(1):1–11.
15. Dearden PK (2006) Germ cell development in the Honeybee (Apis mellifera); vasa and nanos expression. *BMC Dev Biol* 6:6.
16. Dill KK, Seaver EC (2008) *Vasa* and *nanos* are coexpressed in somatic and germ line tissue from early embryonic cleavage stages through adulthood in the polychaete *Capitella sp. I*. *Dev Genes Evol* 218(9):453–463.
17. Bolker JA (1995) Model systems in developmental biology. *Bioessays* 17(5):451–455.
18. Ewen-Campen B, Srouji JR, Schwager EE, Extavour CG (2012) *Oskar* predates the evolution of germ plasm in insects. *Curr Biol* 22(23):2278–2283.
19. Hopf C, Viebahn C, Püschel B (2011) BMP signals and the transcriptional repressor BLIMP1 during germline segregation in the mammalian embryo. *Dev Genes Evol* 221(4):209–223.
20. de Sousa Lopes SMC, Hayashi K, Surani MA (2007) Proximal visceral endoderm and extraembryonic ectoderm regulate the formation of primordial germ cell precursors. *BMC Dev Biol* 7:140.
21. Niehrs C (2010) On growth and form: A Cartesian coordinate system of Wnt and BMP signaling specifies bilaterian body axes. *Development* 137(6):845–857.
22. Bollenbach T, et al. (2008) Precision of the Dpp gradient. *Development* 135(6): 1137–1146.
23. Piepenburg O, Grimmer D, Williams PH, Smith JC (2004) Activin redux: Specification of mesodermal pattern in *Xenopus* by graded concentrations of endogenous activin B. *Development* 131(20):4977–4986.
24. Chen Y, Schier AF (2001) The zebrafish Nodal signal Squint functions as a morphogen. *Nature* 411(6837):607–610.
25. Smith JC (1995) Mesoderm-inducing factors and mesodermal patterning. *Curr Opin Cell Biol* 7(6):856–861.
26. Frasch M (1995) Induction of visceral and cardiac mesoderm by ectodermal Dpp in the early *Drosophila* embryo. *Nature* 374(6521):464–467.
27. Staehling-Hampton K, Hoffmann FM, Baylies MK, Rushton E, Bate M (1994) *dpp* induces mesodermal gene expression in *Drosophila*. *Nature* 372(6508):783–786.
28. Wheeler WM (1893) A contribution to insect morphology. *J Morphol* 8(1):1–160.
29. Roonwal ML (1936) Studies on the embryology of the African migratory locust, *Locusta migratoria migratoides* R. and F. I. The early development, with a new theory of multi-phased gastrulation among insects. *Philos Trans R Soc Lond B Biol Sci* 226(538): 391–421.
30. Vrijens K, et al. (2013) Identification of small molecule activators of BMP signaling. *PLoS ONE* 8(3):e59045.
31. Hayashi K, et al. (2002) SMAD1 signaling is critical for initial commitment of germ cell lineage from mouse epiblast. *Mech Dev* 118(1-2):99–109.
32. Saitou M, Yamaji M (2012) Primordial germ cells in mice. *Cold Spring Harb Perspect Biol* 4(11):a008375.
33. Zeng V, et al. (2013) Gene discovery in a hemimetabolous insect: *De novo* annotation and assembly of a transcriptome for the cricket *Gryllus bimaculatus*. *PLoS ONE* 8(5): e61479.

Supplementary Information for

BMP signaling is required for the generation of primordial germ cells in an insect

Seth Donoughe, Taro Nakamura, Ben Ewen-Campen, Delbert A. Green II, Lory Henderson and Cassandra G. Extavour

correspondence to: extavour@oeb.harvard.edu

This SI file includes:

Detailed Materials and Methods

Animal culture and embryo dissection

Gryllus bimaculatus culture maintenance, embryo collection and injection were performed as previously described (1). After injection, embryos were submerged in 1X phosphate-buffered saline (PBS) with 100 units/ml penicillin and 100 mg/ml streptomycin (VWR 45000-650) and incubated at 29ºC until the desired age. To compensate for potential developmental delays caused by injection, rather than relying on chronological age, control and experimental embryos were dissected at the same developmental stage as judged from the appearance of the egg. Embryos were dissected in 1X PBS and fixed on ice for 1-2h in 4% paraformaldehyde in 1X PBS. Following staining and mounting, the stage of each embryo was confirmed based on embryonic morphology and the progression of developmental events, in order to perform appropriate comparisons between experimental and control embryos.

Cloning and phylogenetic analysis

Primers were designed based on *Gryllus* transcriptome data (2) and *Gryllus* genome data (T. Mito and S. Noji, Tokushima University). PCR amplification of the GC-rich 789 bp *Gb-dpp1* fragment (Table S2) using Advantage 2 Polymerase (Clontech) required the addition of betaine (1M) and DMSO (5%) to the reaction mix. All other gene fragments were amplified using standard PCR conditions. Phylogenetic analyses were conducted as previously described (3). As previously described for analyses of TGFβ family members (4), MUSCLE (5) alignments were edited manually to remove gaps.

In situ hybridization

In situ hybridization was carried out as previously described (1) with the following modifications: *Gb-dpp1* was detected using a mixture of two probes, (555 bp and 789 bp, which overlap by 229 bp, see Table S1), each at 0.1 ng/µL, and hybridized at 65˚C. All other probes were used at 0.5-1.0 ng/µL and hybridized at 70˚C. For double *in situ* and antibody staining, *in situ* hybridization was performed first, followed by immunofluorescence, using standard protocols. *Gb-piwi in situ*/ pMad antibody double-stained embryos (Figure 1a") were imaged as follows: bright-field imaging was used to capture a monochrome image of the NBT/BCIP precipitate; this monochrome image was false-colored, and Photoshop was used to superimpose it onto an image of a single optical section of the fluorescently-labeled antibody captured using a Zeiss Apotome. BMP ligand *in situ*/Gb-Piwi antibody double-stained embryos (Figure 1 d"–f") were imaged as follows: reflectance confocal microscopy was used to capture the ligand transcript signal, laser confocal microscopy was used to capture the Gb-Piwi signal, and optical slices of each marker within 10-20 µm of each other were overlaid using Photoshop.

Immunostaining

Antibody staining was carried out according to standard protocols (6). Primary antibodies used were rabbit anti-Gb-Piwi (3) 1:300, mouse anti-alpha Tubulin-FITC conjugate 1:100 (clone DM1A, Sigma cat. #F2168), goat anti-HRP-Cy3 conjugate 1:100 (Jackson Immunolabs, gift of S. Kunes, Harvard University, USA), rabbit anti-cleaved Caspase 3 1:100 (Cell Signaling # 9661), rabbit or guinea pig anti-Phospho-Smad1/5/8 1:2000 or 1:300, respectively (gift of Dan Vasiliauskas, Susan Morton, Tom Jessell and Ed Laufer, Columbia University, USA). Secondary

antibodies (Invitrogen) were goat anti-mouse 488, goat anti-rabbit 555, goat anti-rabbit 568, goat anti-rabbit 647, goat anti-guinea pig 488, and donkey anti-rabbit 647, used at a concentration of 1:1000. Hoechst 33342 (Sigma) was used at 1:5000 of a 10mg/ml stock solution.

Imaging and image analysis

Images were captured with AxioVision v.4.8 driving a Zeiss Stereo Lumar equipped with an AxioCam MRc camera, or a Zeiss Axio Imager equipped with an AxioCam MRm camera, using epifluorescence either with or without an Apotome. Confocal microscopy was performed with a Zeiss LSM 780 confocal microscope, using comparable gain, offset, and averaging parameters for all samples. For quantitation of pMad expression levels, control and experimental embryos for a given treatment were imaged using identical imaging parameters. Image analyses were performed with AxioVision v.4.8, Zen 2009, Zen 2012 (Zeiss), or ImageJ (NIH). Figures were assembled in Photoshop, InDesign or Illustrator CS4 or CS6 (Adobe).

Statistical analysis

Chi-squared tests were used to compare proportions of embryos without germ cells between RNAi embryos and controls (see Table S3) and proportions of embryos with ectopic PGCs between BMP activator-injected embryos and controls (Figure 3l). To compare distributions of PGC cluster volumes between experimental embryos and controls (Figures 2, 3; Supplementary Figures S5, S6, S8, S9), the Anderson-Darling normality test was first applied to determine whether distributions were normal. Pairs of normal distributions were compared using a two-tailed student's t-test with unequal variance. Pairwise distributions between a normal and a non-normal distribution, or between two non-normal distributions, were performed with the non-parametric Mann Whitney test. Statistical analyses were performed using QI Macros 2013 (KnowWare) in Microsoft Excel.

PGC quantification

Because *Gb-piwi* transcript and protein are cytoplasmic (3), manually counting PGCs in large numbers of embryos proved inefficient. We therefore developed a more efficient method for PGC quantification at the stage when PGCs are assembled into segmentally iterated clusters in A2-A4 (stage 9; 4d AEL). Clusters have an ellipsoidal shape, enabling us to approximate a cluster's volume from the total z-depth of the cluster (Supplementary Figure S4d) and the cross sectional area at the z-depth where the cluster is widest (Supplementary Figure S4b,c). Manual counts of PGC numbers in 24 clusters from wild type embryos revealed that cluster volume was strongly linearly positively correlated with the number of PGCs in a cluster (R^2=0.83; Supplementary Figure S4e), and PGC size was not significantly different between different clusters or wild type and BMP RNAi embryos (Supplementary Figure S4h, i). This allowed us to use PGC cluster volume as an accurate proxy for the number of PGCs in a cluster, and similarly, to use the sum of volumes of all PGC clusters in an embryo as an accurate proxy for the total number of PGCs in that embryo. For each embryo, the segment in which each PGC cluster appeared, and whether it was in the left or the right hemisegment of the embryo viewed dorsally, was recorded. No significant difference was observed between volumes of clusters in the left and right hemisegments of an embryo. See Supplementary Figure S4 for further details on this method. To determine the effect of experimental treatments on PGCs, we used the methods described above to perform three different statistical comparisons: (1) distributions of the sizes of PGC cluster in each segment from experimental and control embryos (as shown in Figures 2g-

k; 3d, e-e', f-f'; Supplementary Figures S5b-f, S6b-f, S8b-g, S9b-g); (2) distributions of the sizes of all PGC clusters that were scored in experimental or control embryos (Supplementary Figures S5a, S6a, S8a, S9a); (3) distribution of the sums of all PGC cluster volumes in experimental and control embryos (Figure 2a, 3g). For the latter comparison, only embryos where PGC clusters were scored in all of abdominal segments A1 through A6 were considered.

RNA interference (RNAi)

Embryonic RNAi on embryos at 0-5h AEL was carried out as previously described (1) for *Gb-dpp1*, *Gb-dpp2* and *Gb-gbb.* Double stranded RNA was injected into the posterior half of each egg. When *Gb-Mad* dsRNA was injected at 0-5h AEL, all embryos arrested in development before 2.5d AEL, when PGCs would first arise in wild type embryos, precluding determination of the effect of *Gb-Mad* RNAi on PGC formation. To overcome the early requirement for *Gb-Mad* in embryonic patterning, we therefore let embryos develop for 24 to 36 hours, allowing them to form a germ band and undergo gastrulation, then reduced *Gb-Mad* activity by injecting *Gb-Mad* dsRNA at 24-36h AEL. For 24-36h AEL embryonic RNAi, eggs were collected in petri dishes of wet sand during a two-hour window, aged in an incubator at 29°C until 24h or 36h AEL, and injected as previously described (1). See Tables S2 and S3 for details of sequences and concentrations of dsRNA used, survival rates and PGC scoring for each experiment.

qPCR validation of RNAi

To validate RNAi using qPCR, whole eggs were homogenized in TRIzol (Invitrogen) and stored at -80°C until RNA extraction. RNA was extracted following the manufacturer's protocol, treated for 30 minutes with 5% TURBO DNAse (Invitrogen), then purified using either phenol chloroform extraction or the TURBO DNA-free Kit (Invitrogen), and used as a template for cDNA synthesis using SuperScript III (Invitrogen). A no-reverse transcriptase control was performed in parallel for each sample, and the resulting cDNA pools were diluted 1:10 in DEPC water. PerfeCta SYBR Green SuperMix (Low ROX, Quanta Biosciences) was used to conduct qPCR reactions in a Stratagene MxP3005 machine. See Supplementary S4 for sequences of primers used for qPCR. The 2-ΔΔCt method (7) was used to compare the relative expression levels of transcripts of interest in RNAi eggs to DsRed RNAi or buffer injected controls, with expression levels normalized to that of *Gb-beta-tubulin*. Each qPCR reaction was performed in triplicate. Supplementary Figure S3 presents mean and standard deviation for each group of three technical replicates.

Identifying mesodermal cells

At 2.5d AEL, the embryo is a bilayered germ band. The only two embryonic cell layers present at this stage are the ectoderm and mesoderm. The ectoderm is the ventralmost layer, and is covered on its ventral side by the extraembryonic amnion. The amnion (and thus the ventral side and ectoderm of the embryo) is unambiguously identifiable based on its large nuclei and squamous cell morphology, and its anatomical position between the ectoderm and the yolk facing the eggshell. Dorsal to the ectoderm (on the side of the ectoderm that is not covered by the amnion) is a single layer of mesodermal cells. The mesoderm is in direct contact with the yolk on its dorsal side. Mesodermal cells are characteristically large and round with large, round nuclei. The identity of this embryonic cell layer as mesoderm and its subsequent morphogenesis to form coelomic pouches and trunk musculature in the thorax and abdomen have been documented in

detail in a variety of short germ insects, including recent works that use conserved molecular markers for mesoderm in *Gryllus* (3, 8-11).

BMP pathway activation

To achieve small molecule activation of BMP signaling, 4′- hydroxychalcone (Santa Cruz Biotechnology Chemicals #SC-262260) was dissolved in DMSO to 10μM or 10mM(12) and injected into eggs at 0-5h AEL, with DMSO injections used as the control. BMP activation was also achieved by injecting recombinant *D. melanogaster* Dpp protein (R&D Systems #519-DP-020/CF) in 4mM HCl to 10 μg/mL or 100 μg/mL into eggs at 0-5h AEL, with 10 μg/mL or 100 μg/mL BSA (New England BioLabs #B9001S) in 4mM HCl as the control.

Some embryos treated with Dm-Dpp displayed an increase in the proportion of S2-S4 segments lacking PGCs. This effect was significant only in A2 for 10 μg/ml Dm-Dpp (Fig S10f), and in A4 for 100 μg/ml Dm-Dpp (Fig. S10h). However, BSA controls also had this effect at 10 μg/ml in A4 (Fig. S10h), and at 100 μg/ml in both A2 and A4 (Fig. S10f, h). Moreover, neither 10 μM nor 10 mM 4-hydroxychalcone treatments caused a significant decrease in PGC formation in any of segments A2-A4 (Fig. S10 f-h). We also noted that PGC formation in A4 was particularly sensitive to any perturbation of the embryos, including injection buffer and DsRed RNAi controls (Fig. S10h). We therefore believe that the loss of some PGC clusters in wild type positions in Dm-Dpp-treated embryos is a non-specific effect rather than revealing that BMP signaling plays a repressive role in PGC formation. Further, the hypothesis that BMP signaling represses PGC formation is not consistent with the supernumerary PGCs and significant increases in ectopic PGCs observed in both BMP activation treatments.

Supplemental Text

qPCR analysis of RNAi treatments

Because *Gb-dpp1* and *Gb-dpp2* show extensive sequence similarity, we wished to test the possibility that RNAi against one of these genes might reduce transcript levels of the other. We therefore performed qPCR assays of *Gb-dpp2* levels in *Gb-dpp1* RNAi embryos (Supplementary Figure S3b), and of *Gb-dpp1* levels in *Gb-dpp2* RNAi embryos (Supplementary Figure S3c).

Gb-dpp1 RNAi was performed with two non-overlapping dsRNA fragments both reduced *Gb-dpp1* transcript levels as expected, but not Gb-dpp2 levels (Supplementary Figure S3a). This confirms that *Gb-dpp1* RNAi specifically knocks down *Gb-dpp1* and not both *Gb-dpp* orthologues. However, both fragments also yielded an increase in *Gb-dpp2* transcript levels at 2.5d AEL, which lessened by 4d AEL but still remained higher than control levels. This could mean that *Gb-dpp1* normally suppresses *Gb-dpp2* levels.

Gb-dpp2 RNAi reduced *Gb-dpp2* levels as expected (Supplementary Figure S3a) and did not affect the levels of *Gb-dpp1*, as assessed with primers amplifying two different non-overlapping fragments of *Gb-dpp1*. This confirms that *Gb-dpp2* RNAi specifically knocks down *Gb-dpp2* and not both *Gb-dpp* paralogues.

Given that *Gb-dpp2* knockdown does not significantly reduce total PGC number per embryo (Figure 2a), we think it unlikely that altered *Gb-dpp2* levels contribute to the PGC reduction seen in *Gb-dpp1* RNAi experiments. We attempted to test this possibility by injecting dsRNA against both *Gb-dpp1* and *Gb-dpp2* into early embryos (see RNA interference section on page 4 of Supplementary Information) at a concentration of 4.5 μg/ml for each gene, the same concentration used for each single gene RNAi experiment. However, in contrast to all of our

single RNAi experiments (Fig. S3a), this double RNAi treatment failed to reduce transcript levels of either *Gb-dpp1* or *Gb-dpp2* at 2.5d AEL (Fig. S3d). Because we were unable to knock down both genes simultaneously at the time of PGC formation, this experiment was inconclusive and did not help us to further resolve the roles of *Gb-dpp1* and *Gb-dpp2* in *Gryllus* PGC specification.

Roles of BMP signaling in germ cells across Metazoa

We surveyed the literature for evidence that BMP signaling was active in and/or required for development of germ cells at some stage of the germ cell cycle across the Metazoa. We considered only gene expression evidence (based on detection of transcript or protein products of BMP pathway members) or functional genetic evidence (based on studies of mutants, RNAi- or morpholino-mediated knockdowns, or applications of pharmacological BMP signaling antagonists or agonists). The results of this survey are summarized in Figure 4b. The following section provides a brief explanation of the evidence for each taxon included in Figure 4b. Taxa are listed in the order shown in Figure 4b.

Hydra *(Hydra vulgaris)* (13) A *Hydra* receptor SMAD is transcriptionally upregulated during oogenesis. Expression remains at this elevated level during germ cell aggregation, nurse cell differentiation, and oocyte differentiation. At the latest stages of oogenesis, transcription returns to lower levels.

Sea anemone *(Nematostella vectensis)* (14, 15) At the planula stage, the *Nematostella* orthologue of BMP2/4 is expressed throughout the gastrodermis, including all eight mesenteries. At this point in development, the two directive mesenteries contain clusters of cells that express Vasa and PL10, and also have characteristic PGC morphology.

Fruit fly *(Drosophila melanogaster)* (16, 17) BMP signaling plays an essential role in maintaining germ line stem cells in the *Drosophila* ovary and testis stem cell niches.

Flour beetle *(Tribolium castaneum* (18-20) At the end of blastoderm stage, a cluster of Vasa-positive cells is found on the inner side of the posterior end of the blastoderm. These cells become a part of the ventral side of the posterior pit as it begins to form. At the same point in development, the *Tribolium* orthologue of BMP2/4 is expressed this tissue (and broadly in the embryo), while pMad is localized to the posterior pit.

Honeybee *(Apis mellifera)* (21) The honeybee orthologue of BMP2/4 is expressed during oogenesis and is localized to the posterior pole of oocytes. pMad is present in the nuclei of follicle cells around the oocyte.

Nematode *(Caenorhabditis elegans)* (22) The *C. elegans* TGF-ß pathway regulates lifetime reproductive capacity by altering many aspects of reproduction, including oocyte fertilizability and oocyte morphology. Loss of function of the *C. elegans* receptor SMAD *sma-2* leads to a reduction in the age-related decline of germ line stem cells.

Oyster *(Crassostrea gigas)* (23) This study identified a TGF-ß protein that does not have clear orthology to other previously identified members of the protein superfamily. This gene is

expressed in the somatic cells that surround oocytes and spermatocytes, at increasing levels as oysters mature.

Lancelet *(Branchiostoma floridae)* (25-27) Lancelet PGCs are specified by germ plasm that is inherited by a single blastomere, which then gives rise to PGCs. At gastrulation and at several subsequent stages of embryogenesis, the PGC-containing tissue expresses the *Branchiostoma* orthologue of BMP2/4.

Colonial tunicate *(Botryllus primigenus)* (24) Germ line precursor cells can develop into both male and female germ cells, and they play an important role in gonad regeneration. Injection of human recombinant BMP4 or BMP2 into the colonial tunicate's vascular system caused an increase in the number of Vasa-positive cells. These Vasa-positive cells formed loose aggregates that were very similar to germ line precursor cells.

Zebrafish *(Danio rerio)* (28) The BMP receptor Alk6b is expressed in zebrafish spermatogonia and early oocytes. A mutation in Alk6b causes abnormal germ cell differentiation.

Axolotl *(Ambystoma mexicanum)* (29-31) Experimental embryological studies established that PGCs are derived the lateral plate mesoderm. Injection of mRNA encoding *Xenopus* eFGF and BMP4 into axolotl embryos caused cells of animal caps explanted from the injected embryos to express the PGC marker *Ax-dazl*.

Rabbit *(Oryctolagus cuniculus)*.(32) In early embryogenesis, BMP2 is expressed in hypoblast and yolk sac cells, immediately adjacent to the epiblast cells where PGCs originate. After BMP2 expression begins, BMP4 is expressed in the mesoderm where PGCs emerge.

Mouse *(Mus musculus)* (33-47) BMP4 and BMP8b are expressed in the extraembryonic ectoderm and BMP2 is expressed in the visceral endoderm. The SMADs are expressed ubiquitously and the receptors are expressed in the epiblast and visceral endoderm. Heterozygous knockouts of the BMP pathway components shown in Figure 4a show reduced or absent PGCs. BMP signaling activates the expression of Blimp1 and Prdm14, which combine to direct subsequent formation of PGCs. BMP4 is also essential for differentiating embryonic stem cells and induced pluripotent stem cells into PGC-like cells.

Author Contributions

S.D. was involved in study design, performed experiments, collected data for and analysed RNA interference experiments and gene expression patterns, and wrote portions of the paper; B.E-C., T.N., D.A.G and L.H. performed experiments, collected and analysed gene expression data and phylogenetic analyses. C.G.E. designed the research, performed experiments, performed analyses of RNA interference experiments and gene expression patterns, collected and analysed immunostaining data, and wrote the paper. All authors discussed the results and commented on the manuscript.

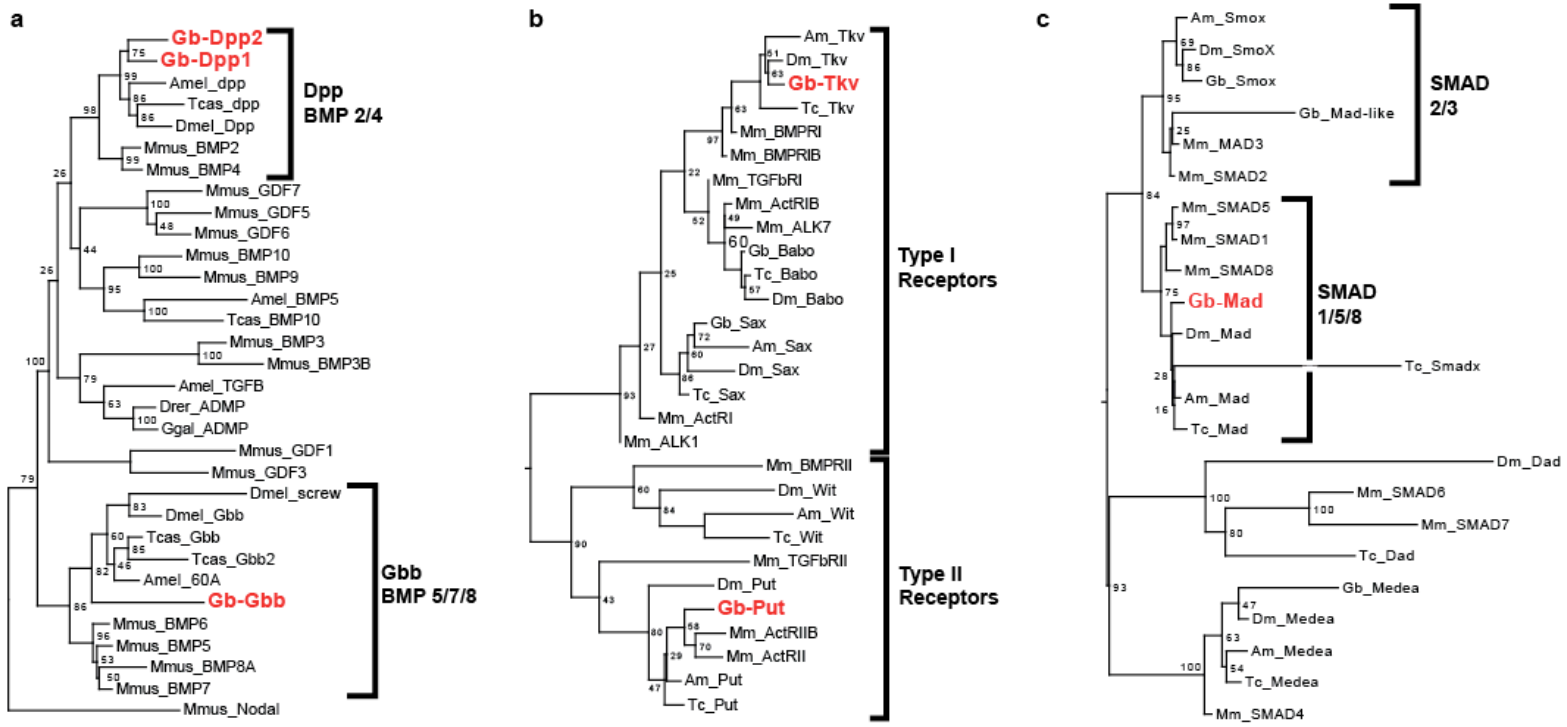

Figure S1. Phylogenetic analysis of *Gryllus* BMP signaling pathway members. Best-scoring maximum likelihood trees are shown, with bootstrap values (2,000 replicates) given as percentages at nodes. **a**, BMP ligands Gb-Dpp1 and Gb-Dpp2 group within the BMP2/4 class, while Gb-Gbb groups within the BMP 5/7/8 class of ligands. **b**, BMP receptors Gb-Sax and Gb-Tkv group with Type I receptors, while Gb-Put groups with Type II receptors. **c**, BMP signaling effectors Gb-Med, Gb-Mad and Gb-Mad-like group with Smad proteins from other animals. *Gryllus* sequences whose expression and/or function were analyzed in this study are indicated in red.

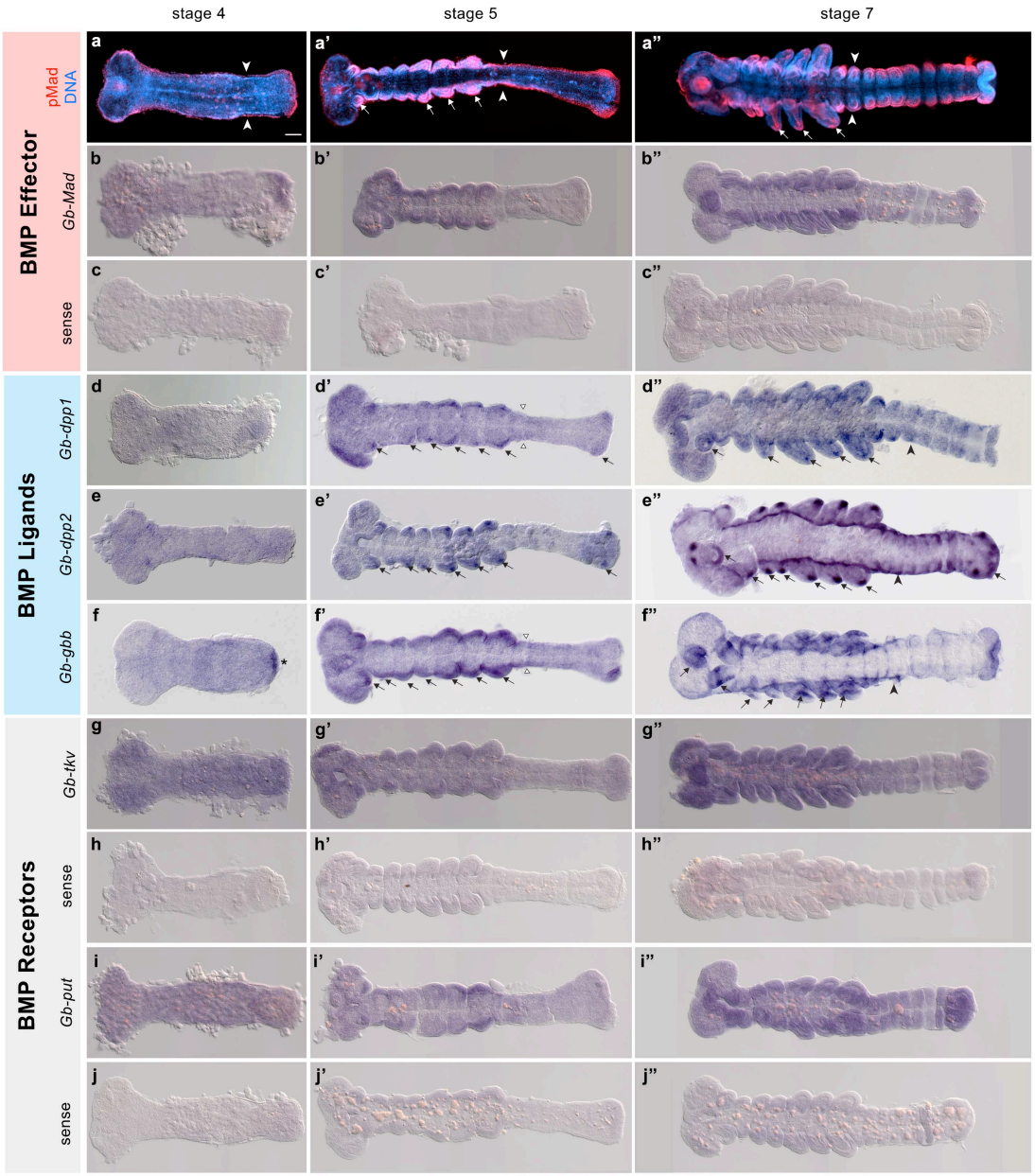

Figure S2. Expression of BMP signaling pathway members throughout mid-embryogenesis in *Gryllus*. a-a", Nuclear pMad is expressed around the dorsal margin of the embryo. Arrowheads indicate dorsal pMad staining in the anterior abdomen, adjacent to and including the region where PGCs will form. pMad is also expressed in the developing appendages (arrows in a', a'"). **b-b",** *Gb-Mad* transcripts are detected ubiquitously throughout stages 4 through 7. **d, e, f,** At stage 4, prior to PGC formation, the BMP ligands *Gb-dpp1*, *Gb-dpp2* and *Gb-gbb* are broadly expressed, although *Gb-gbb* is enriched at the posterior (asterisk in f). **d', e', f',** During stage 5, when PGC specification begins, the ligands are expressed throughout the abdomen. *Gb-dpp1* and *Gb-gbb* expression is slightly enriched at the dorsal margins of the anterior abdomen (arrowheads in d', f'). All three ligands are also expressed at higher levels in appendages and at the posterior (arrows in d', e', f'). **d", e", f",** At stage 7, as PGC clusters are forming, expression of the three ligands is strongest in the dorsal ectoderm of the anterior abdomen (arrowheads), the appendages, the labrum and at the posterior in the case of *Gb-dpp2* (arrows). **g-j",** The receptors *Gb-tkv* and *Gb-put* are expressed ubiquitously throughout stages 4 through 7. Sense controls are shown for each gene that is ubiquitously expressed, showing that the low-level expression of these genes is specific. Anterior is to the left in all panels; scale bar = 100 μm and applies to all panels.

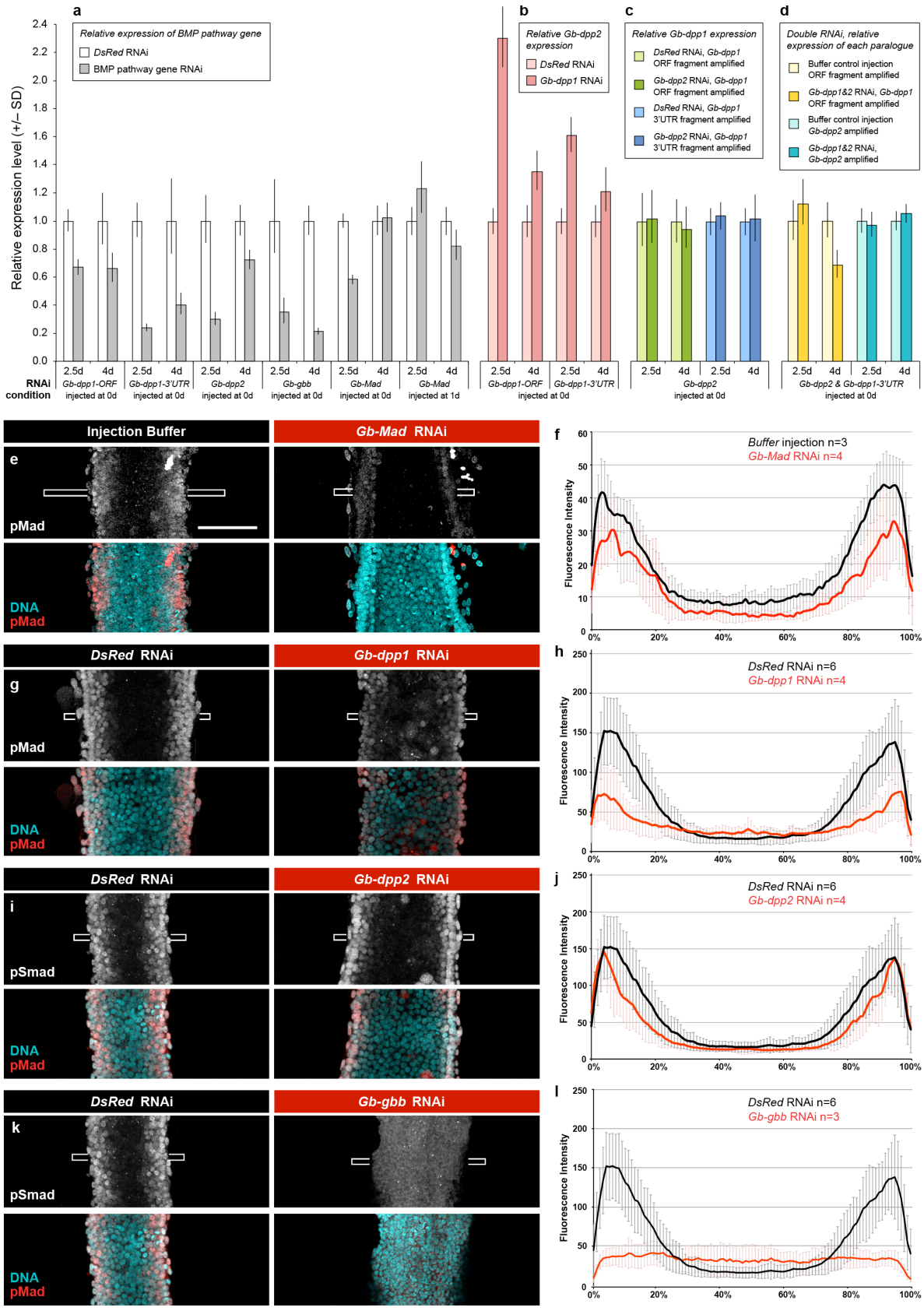
a
Relative expression of BMP pathway gene
DsRed RNAi
BMP pathway gene RNAi
Relative expression level (+/– SD)
RNAi condition
Gb-dpp1-ORF injected at 0d
Gb-dpp1-3'UTR injected at 0d
Gb-dpp2 injected at 0d
Gb-gbb injected at 0d
Gb-Mad injected at 0d
Gb-Mad injected at 1d
b
Relative Gb-dpp2 expression
DsRed RNAi
Gb-dpp1 RNAi
Gb-dpp1-ORF injected at 0d
Gb-dpp1-3'UTR injected at 0d
c
Relative Gb-dpp1 expression
DsRed RNAi, Gb-dpp1 ORF fragment amplified
Gb-dpp2 RNAi, Gb-dpp1 ORF fragment amplified
DsRed RNAi, Gb-dpp1 3'UTR fragment amplified
Gb-dpp2 RNAi, Gb-dpp1 3'UTR fragment amplified
Gb-dpp2 injected at 0d
d
Double RNAi, relative expression of each paralogue
Buffer control injection ORF fragment amplified
Gb-dpp1&2 RNAi, Gb-dpp1 ORF fragment amplified
Buffer control injection Gb-dpp2 amplified
Gb-dpp1&2 RNAi, Gb-dpp2 amplified
Gb-dpp2 & Gb-dpp1-3'UTR injected at 0d
Injection Buffer
Gb-Mad RNAi
e
pMad
DNA
pMad
f
Buffer injection n=3
Gb-Mad RNAi n=4
Fluorescence Intensity
DsRed RNAi
Gb-dpp1 RNAi
g
h
DsRed RNAi n=6
Gb-dpp1 RNAi n=4
Gb-dpp2 RNAi
i
pSmad
j
DsRed RNAi n=6
Gb-dpp2 RNAi n=4
Gb-gbb RNAi
k
l
DsRed RNAi n=6
Gb-gbb RNAi n=3

Figure S3. Validation of RNAi knockdown via qPCR and pMad immunostaining. Quantitative PCR was performed to assess RNAi-mediated gene knockdown at 2.5d AEL (when PGC formation begins) and 4d AEL (when PGC clusters have formed). Bars show relative expression levels normalized to *Gb-beta-tubulin*; error bars represent one standard deviation. **a,** RNAi against all three BMP ligands effectively reduced transcript levels at both 2.5d and 4d AEL. *Gb-Mad* RNAi applied at 0d (0-5h) AEL reduced transcript levels by 2.5d, but expression levels recovered by 4d AEL. *Gb-Mad* RNAi applied at 1d (24-36h) AEL did not appear to significantly reduce transcript levels, but BMP signal activation was reduced in these embryos as assessed with pMad levels, shown in **d** and in Figure 2h. **b**, *Gb-dpp1* RNAi leads to increased *Gb-dpp2* transcript levels (light pink bars) compared to *DsRed* controls (dark pink bars). **c**, *Gb-dpp2* RNAi did not affect *Gb-dpp1* transcript levels, as assessed with two different fragments of *Gb-dpp1* (blue and green bars). **d,** Double RNAi against both *Gb-dpp1* and *Gb-dpp2* results in *Gb-dpp2* levels (turquoise bars) that are comparable to controls, and *Gb-dpp1* levels (yellow bars) that are reduced at 4d AEL but not at 2.5d AEL (See Supplementary Information for details). **e–l,** pMad immunodetection and quantification in RNAi embryos shows that BMP signaling activity is reduced at the onset of PGC specification (2.5d AEL). **e, g, i, k,** pMad expression in segment A3 in representative control and RNAi embryos for *Gb-Mad*, *Gb-dpp1*, *Gb-dpp2* and *Gb-gbb* respectively at 2.5 dAEL. Images of experimental and control embryos were captured with identical confocal microscope parameters. Anterior is up; scale bar = 100 μm and applies to all panels. **f, h, j, l,** Quantified average intensity profiles of pMad levels across the width (X axis: 0-100%) of a 10 μm-wide region through the middle of each of segments A1–A4 (white brackets in **e, g, i, k** indicate this region in A3) of control (black) and experimental (red) embryos. Error bars in **f, h, j, l** represent one standard deviation.

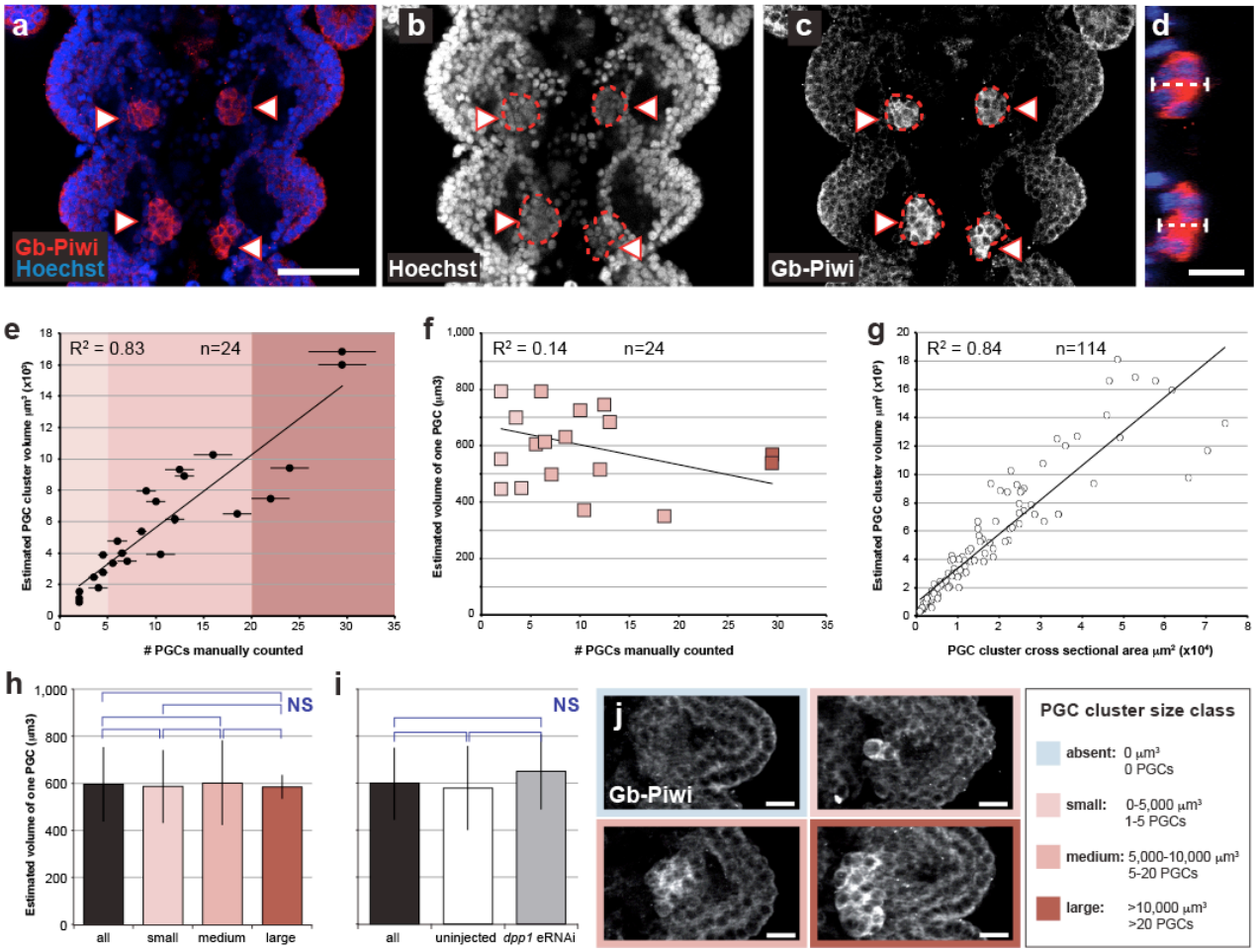

Figure S4. *Gryllus* PGC quantification method. **a–c**, Single optical sections through segments A2 and A3 of a wild type embryo. Arrowheads indicate PGC clusters marked with anti-Gb-Piwi; dotted lines outline the diameter of each cluster at its midpoint on the dorsoventral axis. **d,** y-z orthogonal section through two PGC clusters; dotted lines indicate thickness of each cluster along the dorsoventral axis. **e**, Calculated volume of PGC clusters that spanned the range of observed sizes plotted against the number of PGCs in each cluster (manually counted) shows a strong positive correlation, indicating that cluster volume is a reliable method for quantifying PGCs. Clusters were binned into small (light pink: <5 PGCs; <2,500 μm^3), medium (medium pink: 5-20 PGCs; 2,500–10,000 μm^3), or large (dark pink: >20 PGCs; >10,000 μm^3) categories. **f**, Average calculated volume of a single PGC plotted against the number of PGCs in a clusters (manually counted) shows poor correlation. **g**, PGC cluster volume plotted against cluster cross-sectional area raised to the 3/2 power (to maintain linear proportionality between an area and a volume) shows a strong positive correlation, indicating that cluster growth is generally uniform, i.e. clusters tend to retain an ellipsoid shape as they get larger rather than elongating along any particular axis, although large clusters are more irregular in shape than small clusters. **h**, The average volume of a single PGC (≈600 μm^3) is constant for all cluster size classes. **i**, PGCs have the same volume in uninjected and *Gb-dpp1* RNAi embryos, indicating that PGC reduction phenotypes (see Figure 2; Supplementary Figures S5, S6) are due to reduced PGC number rather than reduced PGC size. Error bars in **h** and **i** represent one standard deviation. **j**, Single optical sections through representative PGC clusters belonging to the four size classes used in Figures 2g-k and 3d, e-e', f-f'. Scale bars = 50 µm in **a** (applies also to **b** and **c**), 20 µm in **d,** 10 µm in **j**.

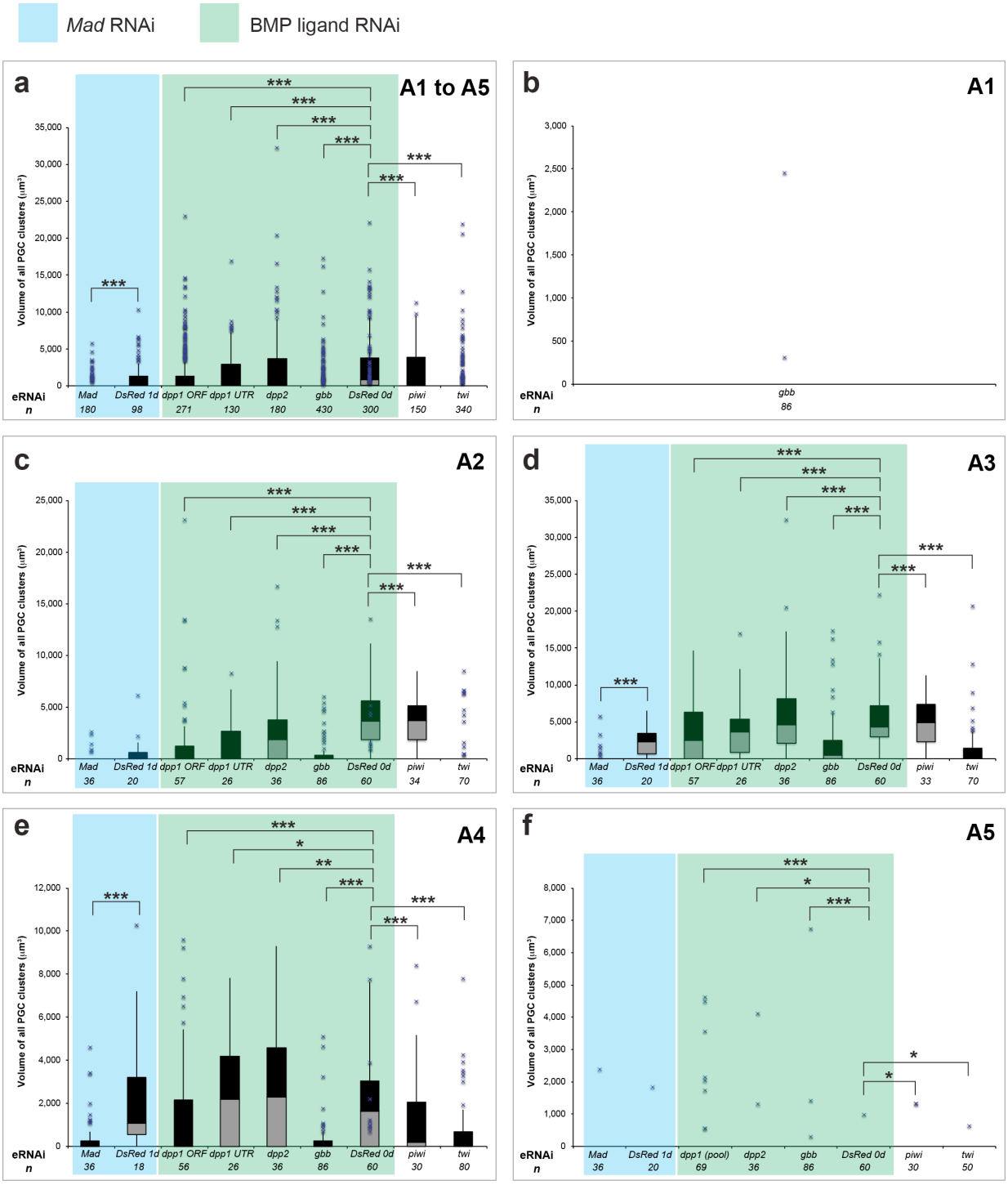

Figure S5. Distributions of all PGC cluster sizes in RNAi treatments. Box-and-whisker plots showing the distribution of volumes of all individual PGC clusters, including absent clusters (volume = 0 µm^3) from all embryos scored in *Gb-Mad* RNAi experiments (blue tint) and BMP ligand RNAi experiments (green tint). Black box: upper quartile; grey box: lower quartile. Whiskers represent the 5th and 95th percentiles. **a**, Distributions of volumes of all clusters scored in segments A1–A5. **b–f**, Distributions of volumes of all clusters scored in a given segment, for segments A1 through A5 respectively. Statistical significance of pairwise comparisons indicated by brackets: *p<0.05, **p<0.01, ***p<0.001. n = number of clusters scored for each condition. These data are summarized in Figure 2g-k, with significance indicated by blue astrices.

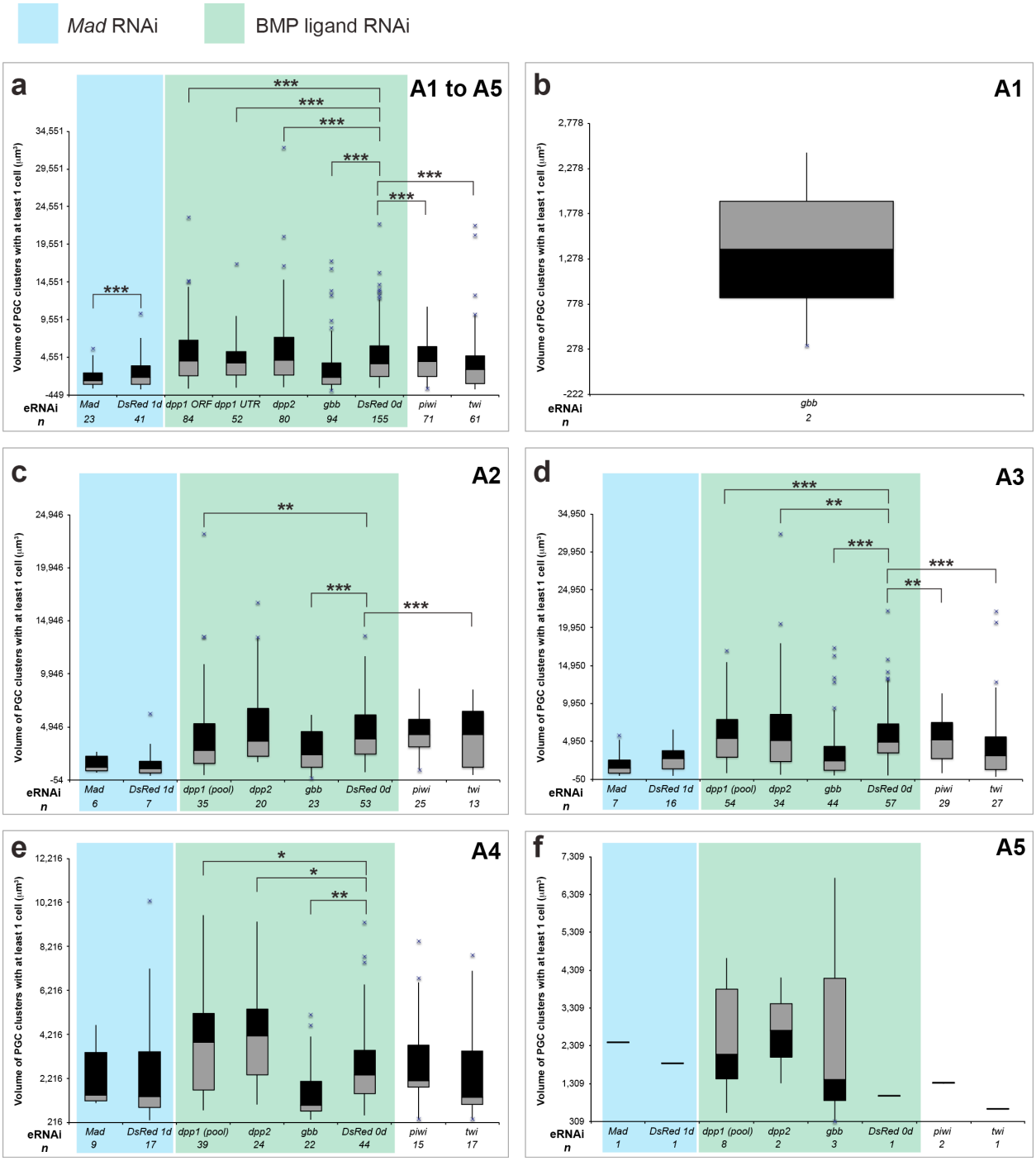

Figure S6. Distributions of non-zero PGC cluster sizes in RNAi treatments. Box-and-whisker plots showing the distribution of volumes of all individual PGC clusters with at least one PGC from all embryos scored in *Gb-Mad* RNAi experiments (blue tint) and BMP ligand RNAi experiments (green tint). Black box: upper quartile; grey box: lower quartile. Whiskers represent the 5th and 95th percentiles. **a**, Distributions of volumes of all non-zero clusters scored in segments A1–A5. **b–f**, Distributions of volumes of all non-zero clusters scored in a given segment, for segments A1 through A5 respectively. Statistical significance of pairwise comparisons indicated by brackets: *p<0.05, **p<0.01, ***p<0.001. n = number of clusters scored for each condition.. These data are summarized in Figure 2g-k, with significance indicated by pink astrices.

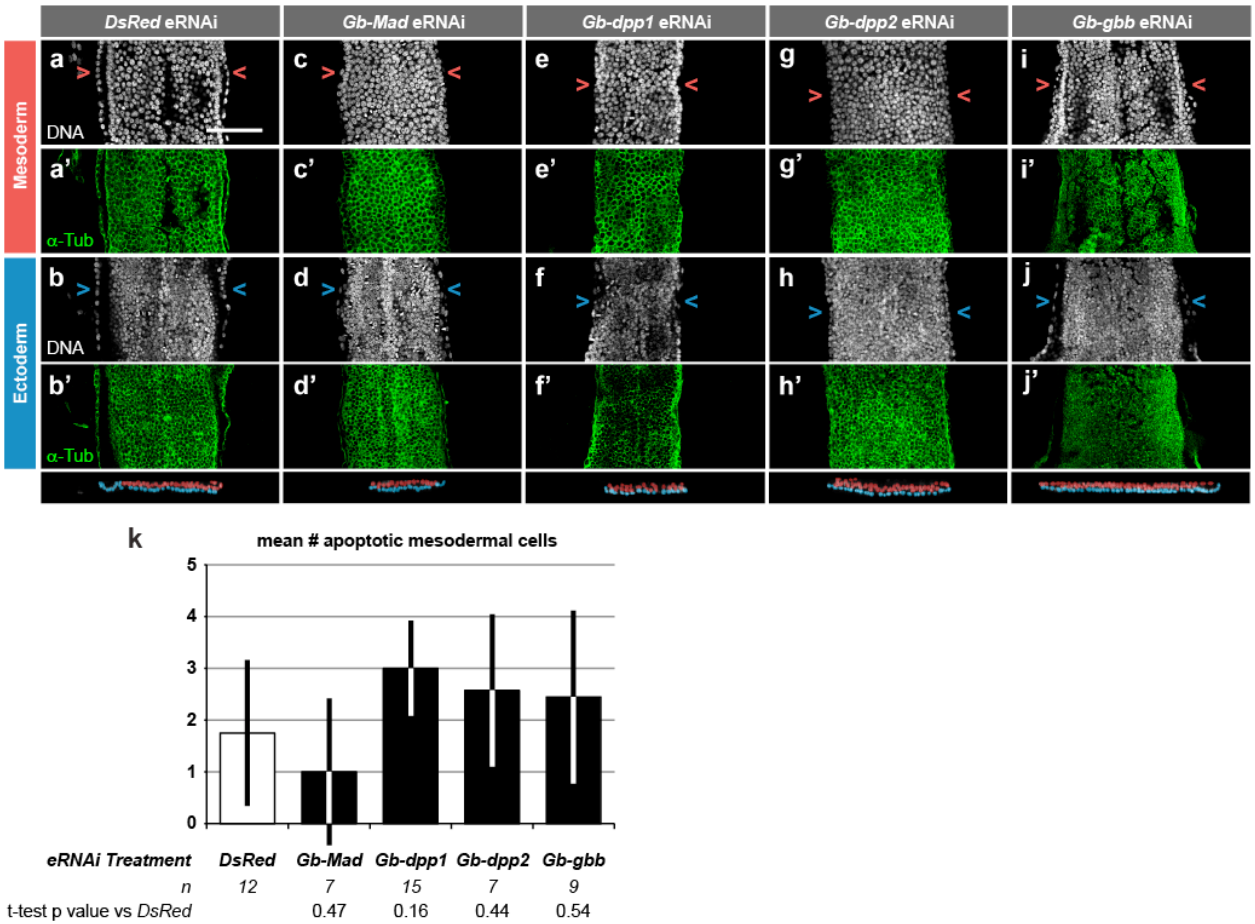

Figure S7. RNAi against BMP signaling pathway members does not abolish mesoderm formation or cause excess mesodermal apoptosis. **a–j'**, 2.5d AEL embryos from each BMP RNAi condition stained with Hoechst (**a–j**) and anti-alpha-Tubulin (**a'–j'**) to visualize distinct cell layers. In wild-type and all RNAi embryos at 2.5d AEL, mesodermal cells have formed a single cell layer immediately dorsal to the ectoderm. Mesodermal cells at this stage can be unambiguously identified by their spatial position (dorsal to the ectoderm) and characteristically large nuclei. Micrographs show a single optical section through segment A3 of representative embryos, at the dorsal (mesodermal) plane (top two rows) and at the ventral (ectodermal) plane (bottom two rows). Bottom row shows orthogonal optical sections through the abdomen of each embryo at the positions indicated by the carets in the panels above, showing contiguous layers of dorsal mesodermal (red) and ventral ectodermal (blue) cells in wild type and all RNAi embryos. Anterior is up in a-l'; dorsal is up in bottom row. Scale bar in a = 100 μm and applies to all panels. **k,** The mean number of apoptotic cells per embryo in control and BMP pathway RNAi embryos, showing no statistically significant difference. Error bars are represent 95% confidence interval.

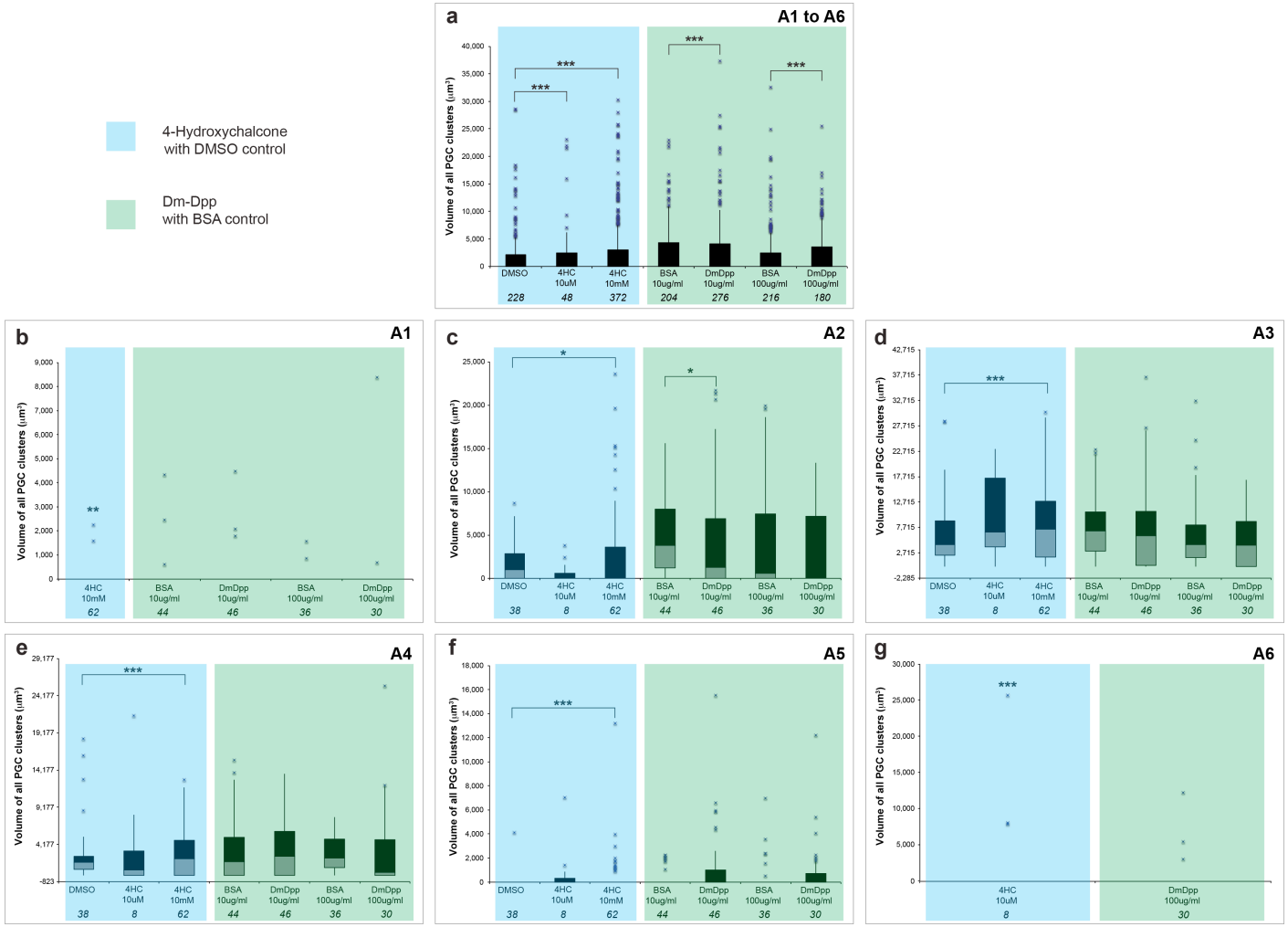

Figure S8. Distributions of all PGC cluster sizes in BMP pathway activation treatments. Box-and-whisker plots showing the distribution of volumes of all individual PGC clusters, including absent clusters (volume = 0 μm^3) from all embryos scored in 4-hydroxychalcone injection experiments (blue tint) and recombinant Dm-Dpp protein injection experiments (green tint). Black box: upper quartile; grey box: lower quartile. Whiskers represent the 5^{th} and 95^{th} percentiles. **a**, Distributions of volumes of all clusters scored in segments A1–A6. **b–g**, Distributions of volumes of all clusters scored in a given segment, for segments A1 through A6 respectively. Statistical significance of pairwise comparisons indicated by brackets: *p<0.05, **p<0.01, ***p<0.001. n = number of clusters scored for each condition. These data are summarized in Figure 3d, e-e', f-f', with significance indicated by blue astrices.

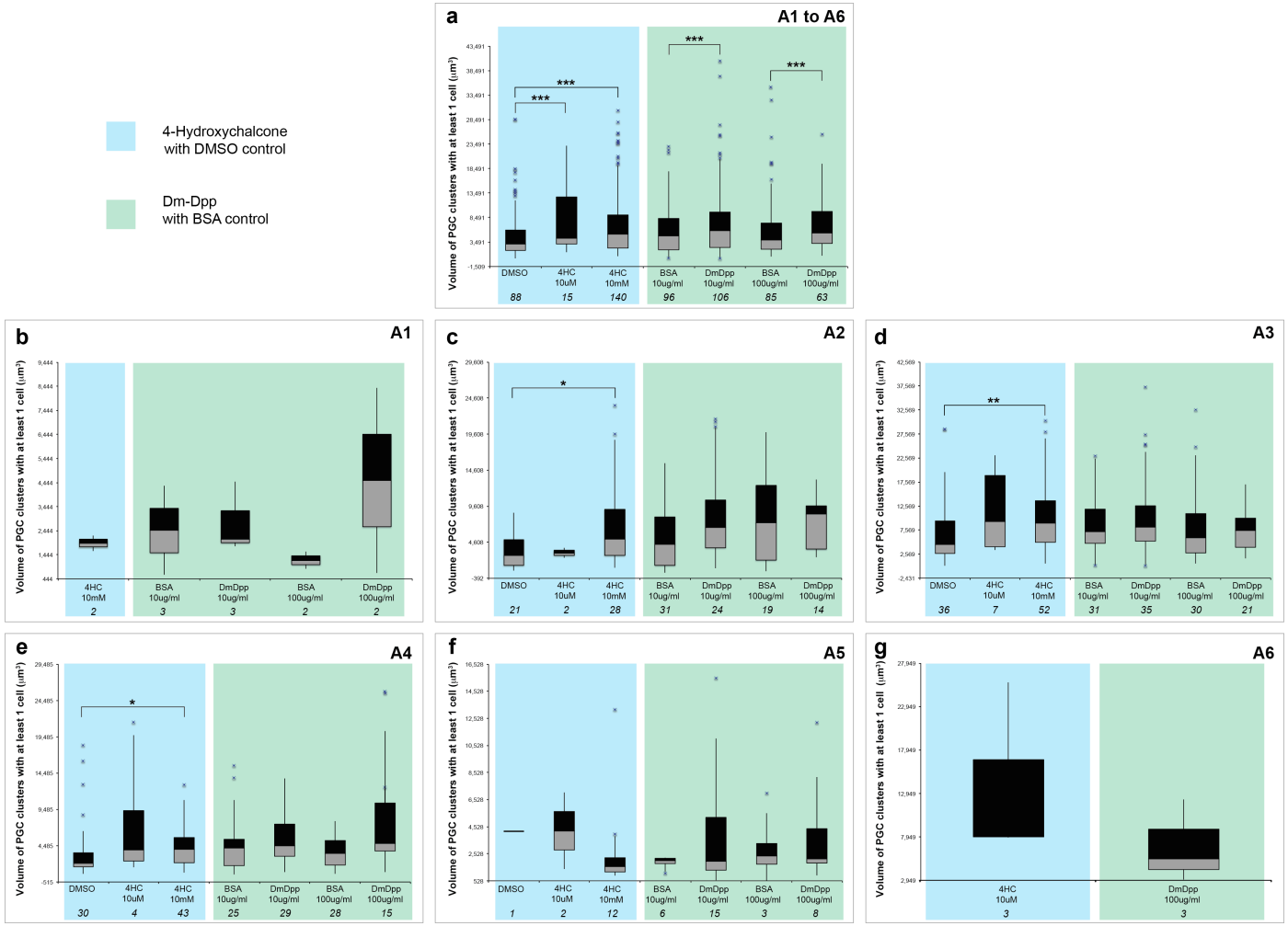

Figure S9. Distributions of non-zero PGC cluster sizes in BMP pathway activation treatments. Box-and-whisker plots showing the distribution of volumes of all individual PGC clusters with at least one PGC from all embryos scored in 4-hydroxychalcone injection experiments (blue tint) and recombinant Dm-Dpp protein injection experiments (green tint). Black box: upper quartile; grey box: lower quartile. Whiskers represent the 5th and 95th percentiles. **a**, Distributions of volumes of all non-zero clusters scored in segments A1–A6. **b–f**, Distributions of volumes of all non-zero clusters scored in a given segment, for segments A1 through A6 respectively. Statistical significance of pairwise comparisons indicated by brackets: *p<0.05, **p<0.01, ***p<0.001. n = number of clusters scored for each condition. These data are summarized in Figure 3d, e-e', f-f', with significance indicated by pink astrices.

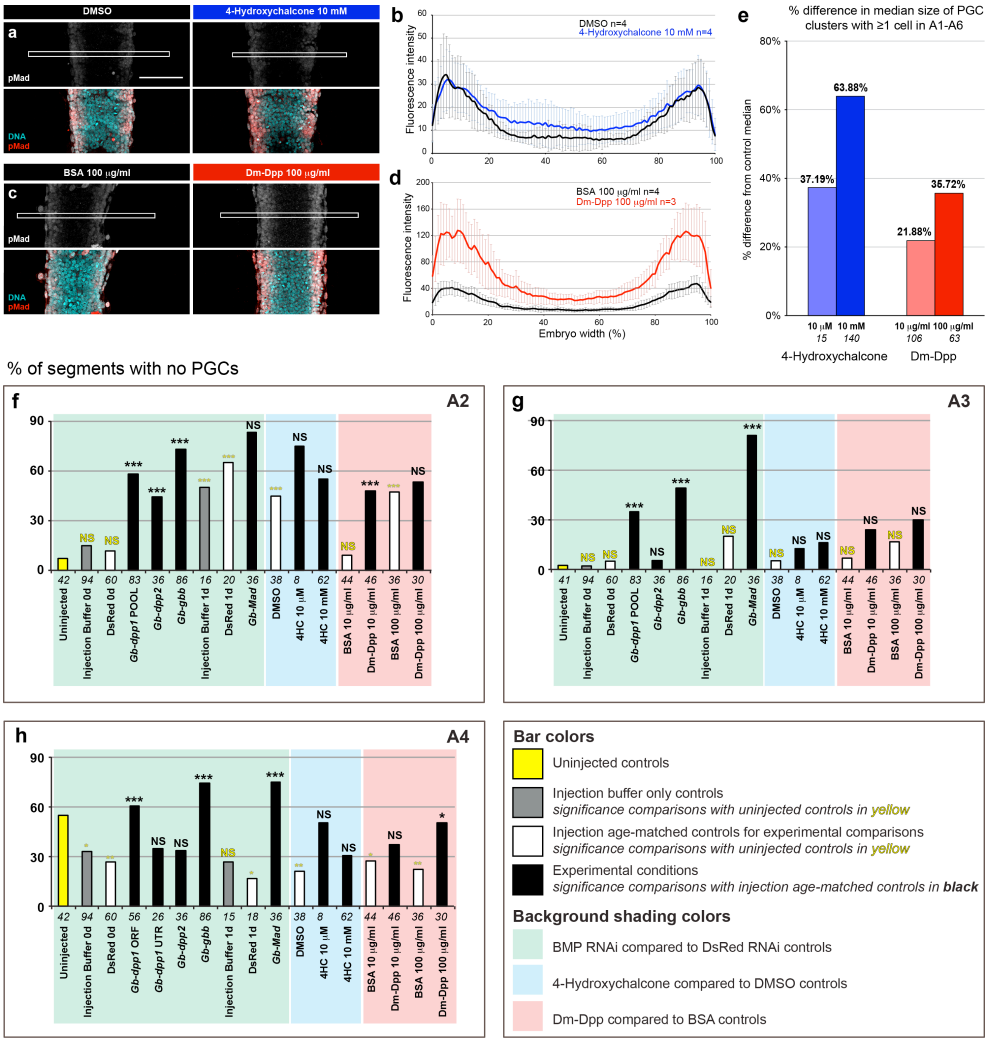

Figure S10. BMP pathway activation leads to elevated pMad levels and a dose-dependent increase in PGC cluster size. a, c, Micrographs showing segment A3 in a representative control and BMP-activated embryo. Anterior is up; scale bar = 100 µm and applies to all panels. **b, d**, Quantified average intensity profiles of pMad levels across the width of a 10 µm-wide region through the middle of each of segments A1–A4 (white brackets in **a** and **c** indicate this region in A3) of control (black) and experimental (blue: Dm-Dpp; red: 4-hydroxychalcone) embryos. Error bars represent one standard deviation. **e**, Both 4'-hydroxychalcone (blue bars) and recombinant Dm-Dpp protein injections had a dose-dependent effect on the median size of PGC clusters with at least one PGC. n = number of clusters scored for each condition. **f-h**, Proportion of segments A2-A4 with no PGCs at all in BMP RNAi embryos with DsRed RNAi, injection buffer and uninjected controls (green background shading), 4'-hydroxychalcone-treated embryos with DMSO controls (blue background shading) and Dm-Dpp-treated embryos with BSA controls (red background shading). In A2 (**f**) and A3 (**g**) the results of two non-overlapping Gb-dpp1 dsRNA fragments were not significantly different and were pooled for this analysis. Statistical significance of comparison of experimental treatments with controls is indicated above experimental (black) bars in black text. The control used for each of these comparisons is the white bar immediately to the left of each set of experiments as follows: DsRed RNAi injected at 0-5h AEL for BMP ligand RNAi; DsRed RNAi injected at 24-36h AEL for Mad RNAi; DMSO injected at 0-5h AEL for 4'-hydroxychalcone injections; BSA at the appropriate concentration injected at 0-5h AEL for Dm-Dpp injections. Statistical significance of these controls (grey and white bars) compared with uninjected embryos (yellow bars) is indicated above control bars in yellow text. Statistical significance calculated using Chi-squared test: NS = not significant; *p<0.05, **p<0.01, ***p<0.001. Numbers in italics underneath each bar indicate sample size.

Gene name	Gene region targeted (1)	length (bp)	Forward primers (5'-3')	Reverse primers (5'-3')
Gb-dpp1	ORF (233 bp) + 3'UTR (556 bp)	789	GCTACGACGCCTTCTACTGC	GGTCGCAATTTTTGCATTTT
Gb-dpp1	ORF	555	GACGTCCTCGAGGGAGAG	GCAGCCACATCCCAGCAC
Gb-dpp1	3'UTR	459	CCCAGTGTAGCTCTGTTTTTG	ACAAAGGCAGCTGAAATCAC
Gb-dpp2	3'UTR	670	TTATGTACGCGTGGATGACG	CGTCTGCTTTCAAAGATCAGG
Gb-gbb	ORF	1458	ATGGCTTGAAGACGAAGAGG	CATGTAAGGCTGCCACAGAA
Gb-Mad	ORF	717	GTCCCCCAGAAGACAGTCAA	AATTCCTGCCTCACGACACT
Gb-put	ORF	721	GCGATTTGGGGCTGTTTAT	GCTGGCCTGATCTTCTTCTG
Gb-tkv	ORF	987	TCATGCAATGCAAAGGTCAC	CCAGCCCCAAAGAGTAAACA

Table S1. Fragments used to make *in situ* hybridization probes. (1) Indicates whether fragment was part of the open reading frame (ORF), 3' untranslated region (3' UTR) or 5' untranslated region (5' UTR).

Gene name	Gene region targeted (1)	length (bp)	Forward primers (5'-3')	Reverse primers (5'-3')
Gb-dpp1	ORF	555	GACGTCCTCGAGGGAGAG	GCAGCCACATCCCAGCAC
Gb-dpp1	3'UTR	459	CCCAGTGTAGCTCTGTTTTTG	ACAAAGGCAGCTGAAATCAC
Gb-dpp2	3'UTR	670	TTATGTACGCGTGGATGACG	CGTCTGCTTTCAAAGATCAGG
Gb-gbb	ORF	1458	ATGGCTTGAAGACGAAGAGG	CATGTAAGGCTGCCACAGAA
Gb-Mad	ORF	717	GTCCCCCAGAAGACAGTCAA	AATTCCTGCCTCACGACACT
DsRed (2)	ORF	678	–	–

Table S2. Fragments used to make dsRNA for RNAi. (1) Indicates whether dsRNA fragment synthesized was complementary to part of the open reading frame (ORF), 3' untranslated region (3' UTR) or 5' untranslated region (5' UTR). (**2)** The coding region of DsRed, a fluorescent protein derived from *Discosoma sp.* was sub-cloned into the pGEM-T Easy vector(1).

Injectant	Injection age (h AEL)	dsRNA Fragment (1)	Concentration	# embryos injected	% (#) embryos survived injection (2)	# embryos scored for PGCs in segments A1-A6 (3)	% (#) scored embryos with no PGCs in entire embryo (4)	# embryos scored for PGCs in segments A2-A4 (5)	% (#) scored embryos with PGCs absent in ≥4 of 6 A2-A4 hemisegments (5)	% (#) scored embryos with fewer PGCs in A2-A4 than lower quartile of control embryos (5)
DsRed dsRNA	0-5	ORF	4.5 µg/µL	503	73.2 (368)	30	0.0 (0)	30	0.0 (0)	26.7 (8)
DsRed dsRNA	24	ORF	4.5 µg/µL	150	68.0 (102)	10	0.0 (0)	10	10.0 (1)	30 (3)
Gb-dpp1 dsRNA	0-5	ORF	4.5 µg/µL	190	81.1 (154)***	19	10.5 (2)	27	51.9 (14)***	55.6 (15)
Gb-dpp1 dsRNA	0-5	3'UTR	4.5 µg/µL	187	84.0 (157)**	13	15.4 (2)	13	15.4 (2)	30.8 (4)
Gb-dpp2 dsRNA	0-5	3'UTR	4.5 µg/µL	177	68.9 (122)	18	0.0 (0)	18	5.6 (1)	22.2 (4)
Gb-gbb dsRNA	0-5	ORF	4.5 µg/µL	532	53.0 (282)***	43	30.2 (13)***	43	65.1 (28)***	79.1 (34)***
Gb-Mad dsRNA	24-36	ORF	3.6 µg/µL	405	63.2 (256)	18	50.0 (9)*	18	77.8 (14)**	88.9 (16)**
BSA	24	–	10 µg/ml	167	75.4 (126)	22	4.5 (1)	20	5.0 (1)	27.3 (6)
Dm-Dpp	24	–	10 µg/ml	161	63.4 (102)*	23	8.7 (2)	23	26.1 (6)	34.8 (8)
BSA	24	–	100 µg/ml	397	59.4 (236)	18	5.6 (1)	18	5.6 (1)	27.8 (5)
Dm-Dpp	24	–	100 µg/ml	464	52.8 (245)	15	6.7 (1)	15	26.7 (4)	13.3 (2)
DMSO	0-5	–	–	267	58.4 (156)	19	0.0 (0)	19	5.3 (1)	26.3 (5)
4'-Hydroxychalcone	0-5	–	10 µM	142	66.2 (94)	4	0.0 (0)	4	25.0 (1)	25 (1)
4'-Hydroxychalcone	0-5	–	10 mM	188	44.1 (83)**	31	0.0 (0)	31	19.4 (6)	9.7 (3)
Injection buffer (6)	0-5	–	–	549	78.5 (431)	59	0.0 (0)	59	1.7 (1)	25.4 (15)
Injection buffer	24-36	–	–	318	92.1 (293)	7	0.0 (0)	7	0.0 (0)	28.6 (2)

Table S3. RNAi, injected protein, and chemical activators used to alter *Gryllus* BMP pathway activity. 1. Indicates whether dsRNA fragment injected was complementary to part of the open reading frame (ORF), 3' untranslated region (3' UTR) or 5' untranslated region (5' UTR). **2**. Embryos were scored as surviving the injection if they were intact and uninfected 24 hours following injection. **3.** Quantitative PGC scoring was performed by allowing embryos to develop to 4-4.5h AEL and staining with the germ cell marker anti-Gb-Piwi(3) (Supplementary Figure S4). The remaining embryos that survived injection were used for qPCR, pMad, morphological or apoptosis analysis. **4.** Includes only embryos in which all hemisegments of A1-A6 were scorable. **5.** Includes only embryos in which all hemisegments of A2-A4 were scorable. **6.** Statistical comparison with injection buffer-only controls indicate that PGC loss in BMP RNAi embryos is not a non-specific consequence of dsRNA injection (see Fig. S10f-h). Asterisks indicate statistical significance relative to controls, calculated using a Chi-Squared test. ***p<0.001, **p<0.01, *p<0.05.

Gene name	Primer pair name	Forward (5' – 3')	Reverse (5' – 3')
Gb-dpp1	dpp1-ORF-qPCR	GTTGGAACGACTGGATCGTG	TGGTTGGTGGAGTTGAGGTG
Gb-dpp1	dpp1-3'UTR-qPCR	GTCTGGAGAGGCTGACGAAC	GGTCGCAATTTTTGCATTTT
Gb-dpp2	dpp2-qPCR	CCATCTGCGTTCTGGAAAAT	CGCAGGTATGCAGTTCCTTT
Gb-gbb	gbb-qPCR	ATATTGGGCTTGTGGCTGAG	AGCCATTCATCCAAAACCTG
Gb-Mad	Mad-qPCR	GCCTCCTAACGTGGAGATGT	TGTAGTTGCACGTTCTTGGTG
Gb-beta-tub	tub-qPCR	TGGACTCCGTCCGGTCAGGC	TCGCAGCTCTCGGCCTCCTT

Table S4. Primers used for qPCR.

References for Supplementary Materials

1. Kainz F, Ewen-Campen B, Akam M, & Extavour CG (2011) Delta/Notch signalling is not required for segment generation in the basally branching insect *Gryllus bimaculatus*. *Development* 138(22):5015-5026.
2. Zeng V, Ewen-Campen B, Horch HW, Roth S, Mito T, & Extavour C (2013) Gene discovery in a hemimetabolous insect: *de novo* annotation and assembly of a transcriptome for the cricket *Gryllus bimaculatus*. *PLoS ONE* 8(5):e61479.
3. Ewen-Campen B, Donoughe S, Clarke DN, & Extavour CG (2013) Germ cell specification requires zygotic mechanisms rather than germ plasm in a basally branching insect. *Curr. Biol.* 23(10):835-842.
4. Van der Zee M, da Fonseca RN, & Roth S (2008) TGFbeta signaling in *Tribolium*: vertebrate-like components in a beetle. *Dev. Genes Evol.* 218(3-4):203-213.
5. Edgar RC (2004) MUSCLE: a multiple sequence alignment method with reduced time and space complexity. *BMC Bioinformatics* 5:113.
6. Patel NH (1994) Imaging Neuronal Subsets and Other Cell Types in Whole-Mount *Drosophila* Embryos and Larvae Using Antibody Probes. *Methods in Cell Biology, Academic Press, Inc.* 44(chapter 24):445-487.
7. Livak KJ & Schmittgen TD (2001) Analysis of relative gene expression data using real-time quantitative PCR and the 2(-Delta Delta C(T)) Method. *Methods* 25(4):402-408.
8. Kainz F (2009) Cell communication during patterning: Notch and FGF signalling in *Gryllus bimaculatus* and their role in segmentation. PhD PhD (University of Cambridge, Cambridge).
9. Wheeler WM (1893) A contribution to Insect Morphology. *J. Morphol.* 8(1):1-160.
10. Roonwal ML (1936) Studies on the Embryology of the African Migratory Locust, *Locusta migratoria migratoides* R. and F. I. The Early Development, with a New Theory of Multi-phased Gastrulation Among Insects. *Philosophical Transactions of the Royal Society of London B. Biological Sciences* 226(538):391-421.
11. Handel K, Basal A, Fan X, & Roth S (2005) *Tribolium castaneum twist*: gastrulation and mesoderm formation in a short-germ beetle. *Dev. Genes Evol.* 215(1):13-31.
12. Vrijens K, Lin W, Cui J, Farmer D, Low J, Pronier E, Zeng FY, Shelat AA, Guy K, Taylor MR, Chen T, & Roussel MF (2013) Identification of small molecule activators of BMP signaling. *PLoS ONE* 8(3):e59045.
13. Hobmayer B, Rentzsch F, & Holstein TW (2001) Identification and expression of HySmad1, a member of the R-Smad family of TGFbeta signal transducers, in the diploblastic metazoan Hydra. *Dev. Genes Evol.* 211(12):597-602.
14. Finnerty JR, Pang K, Burton P, Paulson D, & Martindale MQ (2004) Origins of bilateral symmetry: *Hox* and *dpp* expression in a sea anemone. *Science* 304(5675):1335-1337.
15. Extavour CG, Pang K, Matus DQ, & Martindale MQ (2005) *vasa* and *nanos* Expression Patterns in a Sea Anemone and the Evolution of Bilaterian Germ Cell Specification Mechanisms. *Evol. Dev.* 7(3):201-215.

16. Xie T & Spradling AC (1998) *decapentaplegic* is essential for the maintenance and division of germline stem cells in the *Drosophila* ovary. *Cell* 94(2):251-260.
17. Shivdasani AA & Ingham PW (2003) Regulation of stem cell maintenance and transit amplifying cell proliferation by tgf-beta signaling in *Drosophila* spermatogenesis. *Curr. Biol.* 13(23):2065-2072.
18. Schroder R (2006) *vasa* mRNA accumulates at the posterior pole during blastoderm formation in the flour beetle *Tribolium castaneum*. *Dev. Genes Evol.* 216(5):277-283.
19. Nunes da Fonseca R, von Levetzow C, Kalscheuer P, Basal A, van der Zee M, & Roth S (2008) Self-regulatory circuits in dorsoventral axis formation of the short-germ beetle *Tribolium castaneum*. *Dev. Cell.* 14(4):605-615.
20. Sharma R, Beermann A, & Schroder R (2013) The dynamic expression of extraembryonic marker genes in the beetle *Tribolium castaneum* reveals the complexity of serosa and amnion formation in a short germ insect. *Gene Exp. Patterns* 13(8):362-371.
21. Wilson MJ, Abbott H, & Dearden PK (2011) The evolution of oocyte patterning in insects: multiple cell-signaling pathways are active during honeybee oogenesis and are likely to play a role in axis patterning. *Evol. Dev.* 13(2):127-137.
22. Luo S, Kleemann GA, Ashraf JM, Shaw WM, & Murphy CT (2010) TGF-beta and insulin signaling regulate reproductive aging via oocyte and germline quality maintenance. *Cell* 143(2):299-312.
23. Fleury E, Fabioux C, Lelong C, Favrel P, & Huvet A (2008) Characterization of a gonad-specific transforming growth factor-beta superfamily member differentially expressed during the reproductive cycle of the oyster *Crassostrea gigas*. *Gene* 410(1):187-196.
24. Kawamura K & Sunanaga T (2011) Role of Vasa, Piwi, and Myc-expressing coelomic cells in gonad regeneration of the colonial tunicate, *Botryllus primigenus*. *Mech. Dev.* 128(7-10):457-470.
25. Panopoulou GD, Clark MD, Holland LZ, Lehrach H, & Holland ND (1998) AmphiBMP2/4, an amphioxus bone morphogenetic protein closely related to *Drosophila decapentaplegic* and vertebrate BMP2 and BMP4: insights into evolution of dorsoventral axis specification. *Dev. Dyn.* 213(1):130-139.
26. Zhang QJ, Luo YJ, Wu HR, Chen YT, & Yu JK (2013) Expression of germline markers in three species of amphioxus supports a preformation mechanism of germ cell development in cephalochordates. *EvoDevo* 4(1):17.
27. Wu H-R, Chen Y-T, Su Y-H, Luo Y-J, Holland LZ, & Yu J-K (2011) Asymmetric localization of germline markers Vasa and Nanos during early development in the amphioxus *Branchiostoma floridae*. *Dev. Biol.* 353(1):147-159.
28. Neumann JC, Chandler GL, Damoulis VA, Fustino NJ, Lillard K, Looijenga L, Margraf L, Rakheja D, & Amatruda JF (2011) Mutation in the type IB bone morphogenetic protein receptor Alk6b impairs germ-cell differentiation and causes germ-cell tumors in zebrafish. *Proc. Natl. Acad. Sci. USA* 108(32):13153-13158.
29. Johnson AD, Crother B, White ME, Patient R, Bachvarova RF, Drum M, & Masi T (2003) Regulative germ cell specification in axolotl embryos: a primitive trait

conserved in the mammalian lineage. *Philosophical Transactions of the Royal Society of London. Series B: Biological Sciences* 358(1436):1371-1379.

30. Nieuwkoop PD (1947) Experimental observations on the origin and determination of the germ cells, and on the development of the lateral plates and germ ridges in the urodeles. *Arch. Neerl. Zool.* 8:1-205.
31. Sutasurya LA & Nieuwkoop PD (1974) The induction of the primordial germ cells in the urodeles. *Wilhelm Roux' Archiv. Entwick. Org.* 175:199-220.
32. Hopf C, Viebahn C, & Püschel B (2011) BMP signals and the transcriptional repressor BLIMP1 during germline segregation in the mammalian embryo. *Dev. Genes Evol.* 221(4):209-223.
33. Lawson KA, Dunn NR, Roelen BA, Zeinstra LM, Davis AM, Wright CV, Korving JP, & Hogan BL (1999) *Bmp4* is required for the generation of primordial germ cells in the mouse embryo. *Genes Dev.* 13(4):424-436.
34. Ohinata Y, Ohta H, Shigeta M, Yamanaka K, Wakayama T, & Saitou M (2009) A signaling principle for the specification of the germ cell lineage in mice. *Cell* 137(3):571-584.
35. Hayashi K, Ohta H, Kurimoto K, Aramaki S, & Saitou M (2011) Reconstitution of the mouse germ cell specification pathway in culture by pluripotent stem cells. *Cell* 146(4):519-532.
36. Zhang J & Li L (2005) BMP signaling and stem cell regulation. *Dev. Biol.* 284(1):1-11.
37. Mishina Y, Suzuki A, Ueno N, & Behringer RR (1995) Bmpr encodes a type I bone morphogenetic protein receptor that is essential for gastrulation during mouse embryogenesis. *Genes Dev.* 9(24):3027-3037.
38. Beppu H, Kawabata M, Hamamoto T, Chytil A, Minowa O, Noda T, & Miyazono K (2000) BMP type II receptor is required for gastrulation and early development of mouse embryos. *Dev. Biol.* 221(1):249-258.
39. Ying Y, Qi X, & Zhao GQ (2001) Induction of primordial germ cells from murine epiblasts by synergistic action of BMP4 and BMP8B signaling pathways. *Proc. Natl. Acad. Sci. USA* 98(14):7858-7862.
40. Chang H & Matzuk MM (2001) Smad5 is required for mouse primordial germ cell development. *Mech. Dev.* 104(1-2):61-67.
41. Chu GC, Dunn NR, Anderson DC, Oxburgh L, & Robertson EJ (2004) Differential requirements for Smad4 in TGFbeta-dependent patterning of the early mouse embryo. *Development* 131(15):3501-3512.
42. Vincent SD, Dunn NR, Sciammas R, Shapiro-Shalef M, Davis MM, Calame K, Bikoff EK, & Robertson EJ (2005) The zinc finger transcriptional repressor Blimp1/Prdm1 is dispensable for early axis formation but is required for specification of primordial germ cells in the mouse. *Development* 132(6):1315-1325.
43. Yamaji M, Seki Y, Kurimoto K, Yabuta Y, Yuasa M, Shigeta M, Yamanaka K, Ohinata Y, & Saitou M (2008) Critical function of Prdm14 for the establishment of the germ cell lineage in mice. *Nat. Genet.* 40(8):1016-1022.
44. Ying Y, Liu XM, Marble A, Lawson KA, & Zhao GQ (2000) Requirement of *Bmp8b* for the generation of primordial germ cells in the mouse. *Mol. Endocrinol.* 14(7):1053-1063.

45. Ying Y & Zhao GQ (2001) Cooperation of endoderm-derived BMP2 and extraembryonic ectoderm-derived BMP4 in primordial germ cell generation in the mouse. *Dev. Biol.* 232(2):484-492.
46. de Sousa Lopes SM, Roelen BA, Monteiro RM, Emmens R, Lin HY, Li E, Lawson KA, & Mummery CL (2004) BMP signaling mediated by ALK2 in the visceral endoderm is necessary for the generation of primordial germ cells in the mouse embryo. *Genes Dev.* 18(15):1838-1849.
47. Tremblay KD, Dunn NR, & Robertson EJ (2001) Mouse embryos lacking Smad1 signals display defects in extra-embryonic tissues and germ cell formation. *Development* 128:3609-3621.